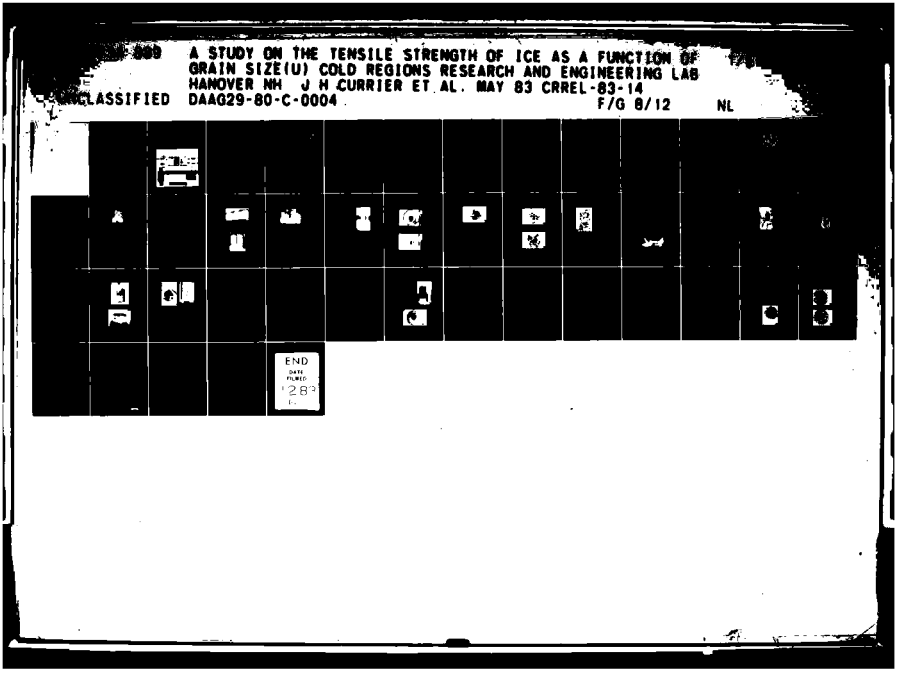
A STUDY ON THE TENSILE STRENGTH OF ICE AS A FUNCTION OF GRAIN SIZE(U) COLD REGIONS RESEARCH AND ENGINEERING LAB HANOVER NH J H CURRIER ET AL. MAY 83 CRREL-83-14
CLASSIFIED DAAG29-80-C-0004 F/G 8/12 NL
END
DATE FILMED
1283

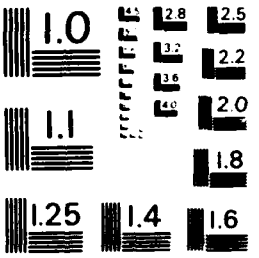

CRREL
REPORT 83-14

A134889

US Army Corps of Engineers
Cold Regions Research & Engineering Laboratory

A study on the tensile strength of ice as a function of grain size

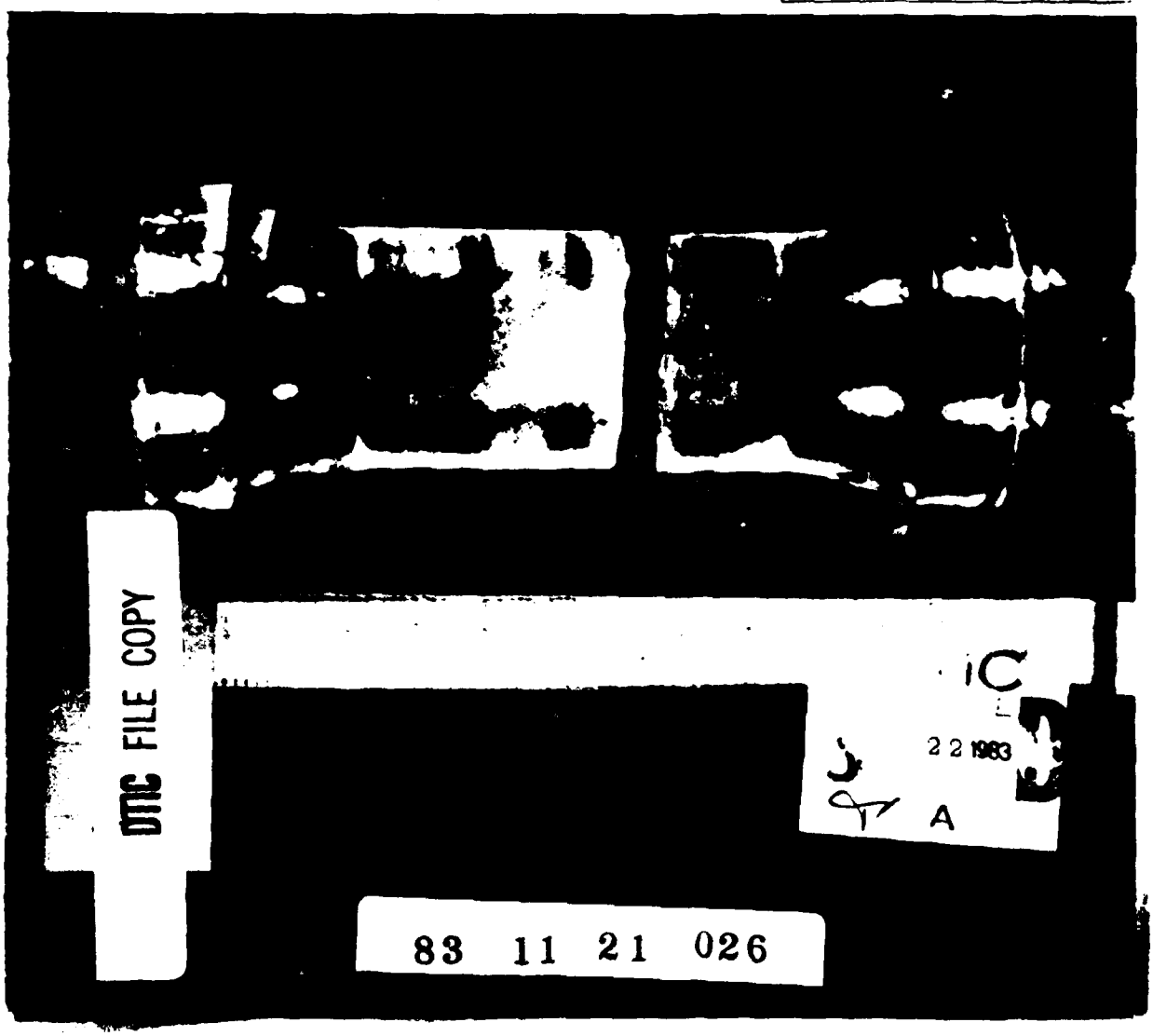

For conversion of SI metric units to U.S./British customary units of measurement consult ASTM Standard E380, Metric Practice Guide, *published by the American Society for Testing and Materials, 1916 Race St., Philadelphia, Pa. 19103.*

Cover: Fine-grained specimen (d = 1.6 mm) after tensile fracture.

CRREL Report 83-14

May 1983

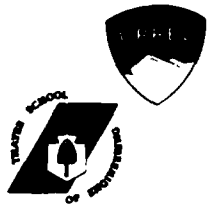

A study on the tensile strength of ice as a function of grain size

J.H. Currier, E.M. Schulson and W.F. St. Lawrence

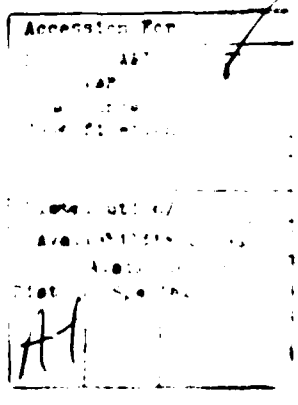

Prepared for
U.S. ARMY RESEARCH OFFICE

Unclassified

SECURITY CLASSIFICATION OF THIS PAGE (When Data Entered)

REPORT DOCUMENTATION PAGE		READ INSTRUCTIONS BEFORE COMPLETING FORM
1. REPORT NUMBER CRREL Report 83-14	2. GOVT ACCESSION NO. AD A134 889	3. RECIPIENT'S CATALOG NUMBER
4. TITLE (and Subtitle) A STUDY ON THE TENSILE STRENGTH OF ICE AS A FUNCTION OF GRAIN SIZE		5. TYPE OF REPORT & PERIOD COVERED 6. PERFORMING ORG. REPORT NUMBER
7. AUTHOR(s) J.H. Currier, E.M. Schulson and W.F. St. Lawrence		8. CONTRACT OR GRANT NUMBER(s) Army Research Office Contract DAAG-29-80-C004
9. PERFORMING ORGANIZATION NAME AND ADDRESS U.S. Army Cold Regions Research and Engineering Laboratory and Thayer School of Engineering, Dartmouth College Hanover, New Hampshire 03755		10. PROGRAM ELEMENT, PROJECT, TASK AREA & WORK UNIT NUMBERS
11. CONTROLLING OFFICE NAME AND ADDRESS U.S. Army Research Office Research Triangle Park, North Carolina 27709		12. REPORT DATE May 1983 13. NUMBER OF PAGES 43
14. MONITORING AGENCY NAME & ADDRESS (if different from Controlling Office)		15. SECURITY CLASS. (of this report) Unclassified 15a. DECLASSIFICATION/DOWNGRADING SCHEDULE

16. DISTRIBUTION STATEMENT (of this Report)

Approved for public release; distribution unlimited.

17. DISTRIBUTION STATEMENT (of the abstract entered in Block 20, if different from Report)

18. SUPPLEMENTARY NOTES

19. KEY WORDS (Continue on reverse side if necessary and identify by block number)

Ductile brittle transition
Ice
Polycrystalline ice
Tensile properties

20. ABSTRACT (Continue on reverse side if necessary and identify by block number)

An analysis of ice fracture that incorporates dislocation mechanics and linear elastic fracture mechanics is discussed. The derived relationships predict a brittle to ductile transition in polycrystalline ice under tension with a Hall-Petch type dependence of brittle fracture strength σ_f on grain size d of $\sigma_f = \sigma_i + kd^{-1/2}$ where σ_i and k are experimental constants. A uniaxial tensile testing technique, including specimen preparation and loading system design was developed and employed to verify the model. The tensile strength of ice in purely brittle fracture was found to vary with the square root of the reciprocal of grain size, supporting the relationship that the theory suggests. The inherent strength of the ice lattice and the Hall-Petch slope are evaluated and findings discussed in relation to previous results. Monitoring of acoustic emissions was incorporated in the tests, providing insights into the process of microfracture during ice deformation.

DD FORM 1 JAN 73 1473 EDITION OF 1 NOV 65 IS OBSOLETE

Unclassified

SECURITY CLASSIFICATION OF THIS PAGE (When Data Entered)

PREFACE

This report was prepared by J.H. Currier, formerly of CRREL and currently an engineer at the ARCO Exploration and Production Research Center, Dr. E.M. Schulson, Associate Professor of Engineering Sciences at the Thayer School of Engineering, Dartmouth College, and Dr. W.F. St. Lawrence, Geophysicist, formerly of CRREL and currently at Polar Alpine Services (Berkeley, California). The original version of this report was a Master of Science thesis prepared by Currier while at the Thayer School of Engineering, Dartmouth College.

The work described was made possible by funding from the Army Research Office, under contract DAAG-29-80-C-004.

There are several individuals to whom the authors express special thanks: David Cole for technically reviewing this report and for his unselfishness and patience in sharing his experience and insights, Stephen Ackley for his major role in initiating and maintaining interaction between CRREL and the Thayer School, Dr. Malcolm Mellor for his advice on testing techniques that helped in the formulation of plans for an important phase of this project, George Lemieux for his personal assistance and the use of his laboratory equipment in the analysis and documentation of specimens, and David Carbee and the personnel of the Soils Laboratory of CRREL for their help and encouragement.

CONTENTS

	Page
Abstract	i
Preface	ii
Introduction	1
Background	2
Development of testing technique	3
Test specimens	3
Tensile testing	15
Compression testing	19
Experimental results	20
Tensile tests	20
Compression tests	24
Discussion	27
Conclusions	30
Suggestions for further work	30
Literature cited	30
Appendix A: Additional information on seed grains	33
Appendix B: Thin-sectioning procedure	35
Appendix C: Displacement transducer calibration	37

ILLUSTRATIONS

Figure

1.	Compressive yield and tensile fracture strengths of a low carbon steel as a function of grain size	3
2.	Ice seed grains from 6.30- to 7.93-mm window	4
3.	Cross section of sample mold	5
4.	Dimensions of dumbbell specimen	5
5.	Domed ice failure near end cap	7
6.	Theorized stress state at end cap resulting in domed fracture surface	8
7.	Specimen end caps	9
8.	Specimen mold partly assembled	9
9.	Sample mold during evaluation/freezing process	10
10.	Fine-grained specimen	11
11.	Wafers of coarse-grained and fine-grained ice showing bubbles	12
12.	Thin section of a fine-grained specimen	13
13.	Thin section of a sample with intermediate-size grains	14
14.	Thin section of sample made with large grains	14
15.	Longitudinal thin section of large-grained sample with refined end zones, after fracture	15
16.	Tensile loading system	16
17.	Tensile testing equipment in environmental chamber ready for testing	18

Figure | Page
18. Compression test equipment ... 19
19. Full cylindrical specimen fractured in tension ... 21
20. Tensile fracture surface revealing cleavage pattern ... 21
21. Photomicrograph of cleaved ice surface ... 22
22. Fine-grained sample with reduced central section ... 22
23. Stress-strain plots for tension tests ... 22
24. Tensile strength vs grain size ... 22
25. σ_f vs $d^{-1/2}$ for tension tests ... 23
26. Tensile stress-strain curve plotted with acoustic emission data ... 24
27. Acoustic emissions in a tensile test compared with AE in control test ... 24
28. Stress-strain curves for compression tests ... 25
29. Tensile stress-strain curve plotted with compression stress-strain curve ... 25
30. Maximum compressive stress vs $d^{-1/2}$ ... 26
31. Compression sample after test ... 26
32. Cross section of a compression sample after test ... 26
33. Stress state near end of sample during compression test ... 27
34. Current results plotted with ranges of earlier data ... 28
35. Typical stress-strain curve showing yield "knee" in compression ... 29

TABLES

Table
1. Comparison of some important physical properties of ice and Synthane ... 6
2. Tensile test data ... 20

A STUDY ON THE TENSILE STRENGTH OF ICE AS A FUNCTION OF GRAIN SIZE

J.H. Currier, E.M. Schulson and W.F. St. Lawrence

INTRODUCTION

The understanding of the behavior of ice in many situations of engineering interest is far from complete. While a great deal of information is available on the creep of ice under relatively low stresses (Mellor and Testa 1969, Colbeck and Evans 1973, Weertman 1973, Homer and Glen 1978), disproportionately little research effort has dealt with the strength and the deformation characteristics of ice subjected to the higher loads ($>10^{-3}$ s^{-1}) that are relevant to many practical engineering applications (Gold 1977, Shoji and Higashi 1978).

The variables that are known to be important to the behavior of ice—temperature, strain rate, strain, porosity, grain structure and surface condition, to name a few—indicate that very complex specifications are needed to fully characterize ice being tested. This characterization is not always complete for the data available, and they often appear contradictory because important variables are not constant between studies. There is a great need now for tests and formulations that can help unify disparate results and improve the fundamental understanding of ice behavior for more effective application to engineering problems.

A new effort in this direction calls for application of the concepts and analyses founded in research on other materials to the study of ice. Undoubtedly the application to ice research of the theory of fracture mechanics (Goodman and Tabor 1978, Schulson 1979), cyclic loading (Mellor and Cole 1981), and acoustic emissions during deformation (Gold 1972, Zaretsky et al. 1979, St. Lawrence and Cole 1982) are contributing significantly to our understanding of the way in which ice behaves.

Further insight into the phenomena involved in ice failure is offered by Schulson (1979), who applied a microstructurally based fracture model, established in metals (Cottrell 1958, Gilman 1958), to hypothesize the brittle to ductile (B/D) transition in polycrystalline ice.

Interest in the brittle to ductile transition in polycrystalline materials developed during World War II when catastrophic failures of welded ship plate caused several Liberty Ships to literally break in two. Near that time and in the decades since, similar failures of steel storage tanks and pressure vessels have prompted more thorough investigations into the service conditions of the materials employed. It is now well known that temperature and loading conditions—especially the effects of stress concentrations—are key factors in the brittle or ductile behavior of steel components, as of course are composition and crystal structure.

Characterization of the transition from ductile to brittle behavior of crystalline materials has primarily focused on metals with body-centered lattice structures and has been viewed in terms of a transition temperature for a given material under given loading conditions, a temperature above which the material is ductile and below which it behaves in a brittle manner.

In the work cited above, Schulson uses dislocа-

tion theory as it applies to ice and the concept of linear elastic fracture mechanics to formulate a hypothesis of the quantitative relationship between grain size, strain rate, and the B/D transition temperature for equiaxed polycrystalline ice under tension. The purpose of the present work is to test experimentally the theory put forth by Schulson. The approach is unique in studies of ice in that it is a systematic investigation of the effect of crystal size on the transition behavior, with a given set of strain rates and temperatures. This leads to a characterization of the phenomenon in terms of what may be regarded as a brittle/ductile transition grain size.

It is important to recognize that in fulfilling this purpose significant advances have had to be made in the technique for testing polycrystalline ice in tension. Problems associated with tensile testing of a truly brittle material are by no means trivial, as has been emphasized by Hawkes and Mellor (1970, 1972) and Haynes (1973, 1978). These researchers are credited with a great deal of effort toward surmounting these difficulties.

The purpose of this research has then been threefold:

1. To adapt and to refine the procedure for preparing polycrystalline ice specimens (developed by Cole [1979] and modified later by Pishvanov [1980]), to a process for reproducibly generating large cylindrical tensile specimens (L = 23.0 cm, D = 9.1 cm).
2. To design and to build equipment for loading the specimens in uniaxial tension on a Materials Testing System machine fitted with an environmental chamber.
3. To carry out tensile tests as needed to characterize the strength behavior of polycrystalline ice as a function of grain size, to test the model proposed by Schulson (1979), and to measure the yield strength in compression, for reasons which will become apparent as the model is presented.

BACKGROUND

The model on which this study is based is developed in detail by Schulson (1979), and will be reviewed here for the reader.

Initially, Schulson's analysis investigates the phenomenon of dislocation pileup in ice grains, and considers the probability of slip propagation into the adjacent grains and of crack nucleation due to stress concentration at the head of the pileup. Established works from the metallurgical literature on brittle fracture (e.g. Eshelby et al. 1951, Cottrell 1958, Smith and Barnby 1967) lead to an evaluation of the requirements for slip propagation and for crack nucleation based on data available for ice. The conclusion is that neither process is significantly more favored than the other under a given stress state.

Given the similar probabilities of slip propagation and crack nucleation, Schulson's investigation then considers whether or not cracks that have nucleated will propagate through the specimen. To address this question, the concepts of both dislocation mechanics and linear elastic fracture mechanics are used. For the first concept, the Hall-Petch relationship shows that

$$\sigma_y = \sigma_i + k_y d^{-1/2} \tag{1}$$

where σ_y = yield stress
σ_i = a measure of the crystal lattice's frictional resistance to slip
k_y = a constant reflecting the extent to which grain boundaries impede slip propagation
d = average grain diameter.

Second, for the fracture toughness concept there is a critical stress intensity factor K_{Ic} above which a crack will propagate through the aggregate:

$$K_{Ic} = Y\sigma_f(\pi C)^{1/2}. \tag{2}$$

where the parameter Y is a geometrical factor determined by crack shape (Y equals $2/\pi$ for lenticular cracks). The tensile stress σ_f is the stress applied in the crack opening mode, and C denotes the half-length of the crack.

If the assumption is made that $2C$ is about equal to the grain size d, then the critical applied stress can be related to other known parameters:

$$K_{Ic} = (2/\pi)\sigma_f(\pi d/2)^{1/2}$$

$$K_{Ic} = (2/\pi)^{1/2}\sigma_f d^{1/2}$$

$$\sigma_f = 1.3K_{Ic}d^{-1/2}. \tag{3}$$

If this critical applied stress for crack propagation is greater than the yield stress ($\sigma_f > \sigma_y$), then the material behaves in a ductile manner. If the converse is true ($\sigma_f < \sigma_y$), then brittle behavior results. Since the expressions for both σ_y and σ_f are dependent upon the grain size of d, eq 1 and 3 can be equated to give a critical grain diameter d_c:

$$d_c = \left(\frac{1.3K_{Ic} - k_y}{\sigma_i}\right)^2 . \quad (4)$$

This result is analagous to, and may be best displayed by, the work of Low (1954). Figure 1 shows tensile fracture stress and compressive yield stress as a function of the square root of the reciprocal of grain size in a low carbon steel. At grain diameters greater than a critical value, the tensile strength lies along the line described by the yield stress plot. As grain diameter becomes smaller than d_c, the tensile strengths exceed the yield stress by progressively greater amounts.

Investigating the elements of eq 4 as they apply to ice, one can relate the inherent lattice slip resistance σ_i to both strain rate and temperature through the expression (e.g. Muguruma 1969)

$$\dot{\epsilon} = A\sigma_i^n e^{-\Delta H/kt} \quad (5)$$

where $\dot{\epsilon}$ is strain rate in s^{-1}, T is the temperature in kelvins, k is Boltzmann's constant, and A, n and H are experimental constants. If σ_i from eq 5 is substituted into eq 4, the result is a relationship between critical grain size, strain rate and temperature:

$$d_c = A^{2/n}\left(\frac{1.3K_{IC} - k_y}{\dot{\epsilon}^{1/n} e^{\Delta H/nkT}}\right)^2 . \quad (6)$$

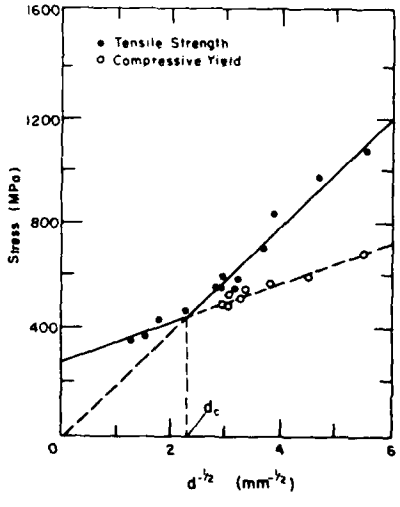

Figure 1. Compressive yield and tensile fracture strengths of a low carbon steel as a function of grain size (after Low 1954).

Using data available, Schulson evaluates this expression over ranges of these test parameters to establish a basis for experimental investigation. A laboratory program using a newly developed tensile testing technique was performed to verify the relationship indicated by this quantitative model.

DEVELOPMENT OF TESTING TECHNIQUE

Test specimens

Tests were carried out on ice specimens fabricated in the laboratory using the vacuum technique developed at CRREL by Cole (1979). This technique was modified by Pishvanov (1980) to produce large cylindrical samples 23.1 cm long and 9.1 cm in diameter. His modifications were employed in this study to make specimens of these same dimensions.

In Cole's method the equiaxed, random nature of the polycrystalline aggregate is achieved by packing a cylinder with ice grains of the appropriate size, evacuating it, flooding it with distilled water, de-airing and then freezing the liquid in the voids between the existing crystal seeds. The details of the procedure are as follows.

Seed grains

Seed grains for these experiments had diameters of 0.42 to 12.7 mm in 12 sieve window categories (App. A). Specimen seed grains smaller than 2 mm were obtained by crushing harvested snow through a sieve and allowing the crystals to segregate into graduated size ranges on smaller sieves below. In a given size window the variation from average was kept to about ±10%, as the uniformity of the crystal diameters is an important factor when correlating mechanical properties with grain size. An important exception to this uniformity is the large window of d = 0.42 to 0.83 mm, which matches the seeds used in studies by Hawkes and Mellor (1972), Haynes (1973), Cole (1979) and Pishvanov (1980).

It is noted that in the Hawkes and Mellor (1972) study, where ice was seeded with sieved snow, the range of seeds for a given sample was not tightly controlled. Although the specimens were fine-grained (d < 1 mm) so that absolute differences between seeds were not great, relative differences were as great as a factor of two. Assuming that grain size is an important parameter in the brittle fracture of ice, then the concern should be that the largest grains present, offering larger slip planes for dislocation pileups, may dictate the behavior, independent of the actual average grain diameter.

Figure 2. Ice seed grains from 6.30- to 7.93-mm window. Numbered units at top are in centimeters. Note the uniform size and the faceted surfaces of the crystals.

Therefore, it must be recognized that, although polycrystalline ice of a highly uniform grain size may not be common in nature, careful specification of the crystal size is needed for the purposes of testing hypotheses in which grain diameter is a key variable. The relatively larger window for very fine sieved snow was used here in attempting to reproduce the material tested in the earlier work, which apparently had a quite uniform grain size.

Interesting observations came from the large samples seeded with snow in the 0.42- to 0.83-mm range. Anomalous grain growth occurred both during fabrication and after straining. For details of these findings, as well as a correlation of the grain size produced by each seed window, the reader is referred to Appendix A.

Seed grains larger than 2 mm were made from ice sheets frozen on pans of distilled water. Stainless steel holding pans were chosen over containers made of other materials, as conductivity tests showed no contribution from the stainless steel to the electrolytic impurity content of the water. A slow freeze (0.5 cm/hr) in a room at 0°C allowed air and other impurities to be pushed ahead of the freeze front and their concentrations in the ice sheet to be kept at a low level. The water depth was kept much greater than the thickness of the ice sheet to be grown, giving a large volume of liquid to dilute impurities excluded from the ice as it formed. A ratio of water depth to ice cover was arbitrarily chosen as 10. It was observed that this water depth also produced ice that was almost entirely free of air bubbles. Thin-section analysis (discussed more thoroughly later) of resulting ice sheets showed large crystals extending through the thickness of the sheet and covering areas on the order of 100 cm^2. Thus when the ice sheets were removed from the pans and broken into pieces of $d < 10$ mm it was well assured the vast majority of pieces would be single crystals.

Ice subcrystals were produced by pounding the sheets through a grate and sieving the pieces in standard soil sieves. As with the smaller grains produced from snow, the sieves were sized to give uniformity of $\pm 10\%$. (The 2.4- to 4.0-mm window was larger because the intermediate sieves were not available). The resulting ice grains were in general equiaxed and very faceted (see Fig. 2).

Since the seed grain material was obtained from different sources, an effort was made to ensure that the source material did not represent a hidden variable in the specimens. Conductivity tests were run on samples of meltwater from the seed grains and resulting ice to determine electrolytic impurity contents. Measurements were made using a Leeds and Northrup conductivity probe and bridge, with all readings normalized using a compensation factor to 25°C. The fine snow grains had a conductivity of 9.4×10^{-6} ohm^{-1} cm^{-1}, while larger grains obtained from ice sheets showed an average value of

3.3×10^{-6} ohm^{-1} cm^{-1}. The distilled water used in all phases of the preparation process was from a distillation system lined with tin throughout, and had a conductivity of 1.5×10^{-6} ohm^{-1} cm^{-1}. The specimens showed very similar conductivities regardless of the seeds. The fine-grained samples' conductivity was 6.0×10^{-6} ohm^{-1} cm^{-1} and the value for the coarse-grained was 5.5×10^{-6} ohm^{-1} cm^{-1}. Thus it was concluded that the purity of the samples did not vary significantly with the source material used.

As a reference, the conductivity value of the fine-grained samples, 6.0×10^{-6} ohm^{-1} cm^{-1}, corresponds to 2.5 ppm NaCl, if, as is commonly assumed, this salt makes the total contribution to the ion concentration (Otten 1972).

Molding equipment

The mold used by Pishvanov (1980) was employed in the present work, as well as a similar one manufactured with several modifications needed for tensile specimens (see Fig. 3). Both were 6061 aluminum cylinders split into halves longitudinally with the matching faces machined and polished to facilitate a tight seal. Bolts along each seam, aligned tangentially to the cylinder, fastened the halves together securely. It was found that large external clamping rings near each end of the cylinder improved the vacuum seal and thus were employed as well.

For tensile specimens which required a reduction in area of the gauge length (further discussion of necked specimens is found in *Specimen Production* below), an acrylic (Lucite) sleeve, split into halves, was inserted into the center of the assembled aluminum cylinder and fixed there to make a dumbbell-shaped chamber. The dimensions of the sleeve and of the modified chamber are shown in Figure 4. The acrylic material was chosen for this application partly for ease of machining, but primarily for its thermal conductivity, which allows it to substitute for a volume of ice-water mixture without significantly perturbing the cylindrical freeze front.

Proper alignment of the end caps perpendicular to the axis of the cylinder is essential, especially for tensile samples. This alignment is achieved by two carefully machined aluminum alignment rings, each of which was fastened to the outside face of an end cap and then held in a fixed post-

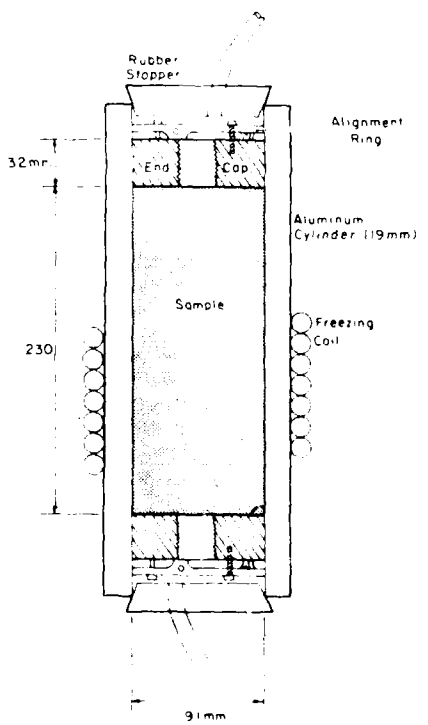

Figure 3. Cross section of sample mold.

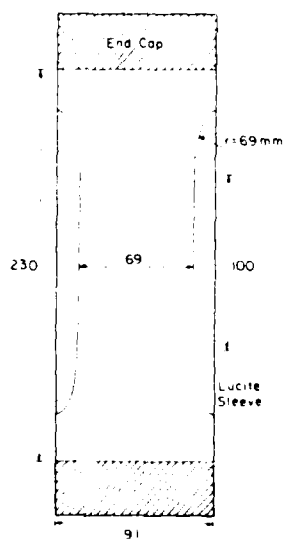

Figure 4. Dimensions of dumbbell specimen.

tion in the cylinder by three screws extending radially through the cylinder wall. It is in this position that the end caps become integral parts of the specimen as it is formed, assuring tightly controlled alignment for testing.

End caps

The specimen end caps were machined from sheets of a composite formed by phenolic resin impregnating layers of linen (Synthane). An effort was made to keep the end cap material as compatible as possible, thermally and elastically, with the ice to minimize stress at the interface. Table 1 compares some important physical properties of ice and Synthane.

Table 1. Comparison of some important physical properties of ice and Synthane.

	Synthane	*Ice*
Coefficient of thermal expansion (α)	3.0-4.0 × 10⁻⁵/°C	5.4 × 10⁻⁵/°C
Young's modulus (E) (at 0°C)	6.2-9.6 GPa	8.6 GPa
Poisson's ratio (ν)	0.35	0.33
E/ρ	22.6 GPa	25.8 GPa

While the end caps used by Pishvanov (1980) for compression tests were 19 mm thick, uniaxial tensile stresses applied in the current series of tests required thicker, more rigid caps. Both molds were made to accommodate 32-mm-thick end caps without compromising the L/D ratio of >2.5 in the original design.

Precise fabrication of the end caps is essential to the effectiveness of the aligning technique involving the retaining rings in the cylinder. The machining steps used in making an end cap are as follows.

A rough disc was cut from phenolic sheet on a band saw. This was held flat on a milling machine table and a center hole drilled and reamed to a 19-mm diameter. An arbor was fitted very tightly into the hole and held on a lathe spindle in a collet. The circumferential surface of the cap was turned down to the final size of D = 9.1 cm. Next the disc was held in a six-jaw lathe chuck, and the center hole enlarged and threaded to 1 in.-14 threads, with tools held in line on the lathe tail stock. Without shifting the disc in the jaws, the outward face of the disc was tooled slowly to a smooth surface perpendicular to the threaded center hole. Next the disc was reset in the chuck with the opposite face outward. This face was first tooled smooth and perpendicular to the spinning axis, and then roughened by quickly passing a single-point threading tool across it, making circumferential grooves and plucking cotton fibers out of the laminate. A few trials on scrap surfaces determined which relative speed and depth of cut on the tool produce a surface of desired roughness.

In the final step the cap was removed from the lathe chuck and mounted on a milling machine table in an indexing head, the smooth face upward. Three threaded (6-32) holes spaced at 120° to one another were machined around the perimeter. These holes would accept the screws by which the alignment ring was fastened.

Prevention of end failure

Developmental tensile testing was done using end caps with the inside (ice interface) tooled to a rough surface as described above. Preliminary tests of the tensile strength of an ice bond with this surface were carried out using simple cantilever beam tests and the results showed consistent strengths of 2 MPa.

A number of tensile tests on actual specimens showed that the adhesion at the ice/end cap interface was not a weak link in the system, as nearly all tests produced fractures that occurred entirely in the ice. However, all of these fractures did occur very near to one of the end caps, and in most cases the break formed a shallow dome and dish with a flat annular perimeter. A typical fracture surface of this sort is shown in Figure 5. Although such failures were not deemed satisfactory for obtaining tensile strength data, they do yield some important information.

First, these fractures were radially symmetric, which is in itself an indication that the stress applied to the specimen was indeed uniaxial as intended. Misaligned loading would be expected to result in a fracture that was, if not noticeably biased, at least less symmetric than the domed paths produced.

Further evidence of axial loading was the nature of the fracture surface itself. Being transgranular cleavage fractures, the paths the cracks followed can be retraced by careful inspection of the pattern left on the grains. As a crack propagates through a grain, it is energetically more favorable to travel along certain of the crystallographic planes than others. When the crack tip reaches a neighboring grain in the polycrystal, those favorable planes have different orientations in space. The crack must in effect "search for" its preferred

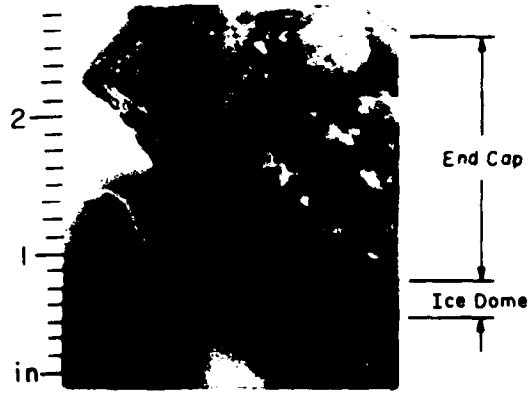

Figure 5. Domed ice failure near end cap.

path dictated by the applied stress and the energy required to cleave available planes. The crack may locally change directions and planes a number of times before arriving at a plane on which it can relatively easily pass through the remainder of that crystal. This leaves the impression of a river pattern with many tributaries emanating from the side of the grain first reached by the crack.

By piecing together in this manner the paths that the fracture followed, it was apparent that the crack or cracks started near the surface of the sample and established the planar annulus around the perimeter of the cross section first, then propagated from many points around the edge and up over the dome to a point near the center of the sample.

The evidence that the dome formed by cracking from many directions shows that the stress acting at any one point on the circumference of the cross section is not significantly greater than at other points. The consistent occurrence of the fractures near one of the end caps indicates complication in the stress state due to the ice/end cap interface. In conjunction with this indication, the annulus-and-dome-shaped failure surface leads to the following theory of the nature of the problem at the end cap grips.

Recognizing that elastic and thermal properties of ice or of an anisotropic laminate such as Synthane cannot be precisely specified, it is assumed that the values of the elastic moduli and/or thermal expansion coefficients do not match perfectly so that there is a differential at the interface where the end cap grips the ice. Since the ice/Synthane bond occurs at a temperature very close to 0°C and the sample must be equilibrated to a test temperature of −10°C, differential thermal contraction causes a shear stress at the interface. While this alone is not enough to cause failure, an applied tensile stress causes differential lateral contraction, superimposing an additional shear stress at the boundary. At some point in the tensile test, the combination of these effects reaches a critical level where the shear component contributes enough to the stress state to cause a crack to propagate. The shear will be at a maximum near, but not at, the outer edge of the interface, which follows from an analysis presented by Hawkes and Mellor (1970) for uniaxial compression on cylinders with radial restraint of the end planes. Thus the crack starts near the perimeter of the sample. While the maximum stress acts right at the ice/end cap interface, the adhesive resistance offered by the indistinct interface causes the crack to travel just inside the ice very near the end cap. This reasoning is supported by the 1 to 2 mm of ice cover remaining on the edge of the end cap face.

As the fracture proceeds inward some distance, the effective cross-sectional area of the specimen is reduced and the tensile stress increases to the point where a crack can propagate away from the interface and is not restricted to the zone of maximum shear stress. Now the fracture, propagating in the crack opening mode, travels perpendicular to the

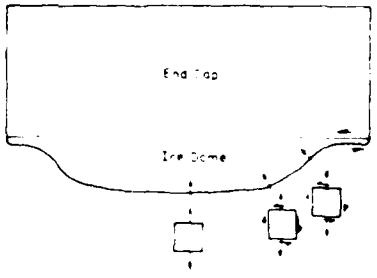

Figure 6. Theoretical stress state at end cap resulting in domed fracture surface.

direction of the maximum principal stress. This direction describes a curve, as the shear component decreases from a finite value at the outside of the remaining cross section to zero at the center of the specimen. If, as indicated in Table 1, E of the end cap is less than that of ice (i.e. the end cap is more compliant), the shear stress due to tension on the system will act radially inward in the specimen leading to a dome-shaped ice cover adhering to the end cap after fracture (see Fig. 6).

If this theory is a valid one, then the problem of the mismatch at the interface could have one of two solutions. First, an interfacial layer could be included in the bond that was compliant and therefore would not transmit the shear stress responsible for the end zone fracture. Second, the resistance to cracking across the ends could be increased by extending the rough interface farther into the sample than afforded by the simple plucking method.

The first step taken to solve the interface mismatch problem was to incorporate both concepts. A 3-mm sheet of gasket rubber was epoxied to the end cap and then jute-backed nylon carpet was epoxied to the rubber. It was essential that the tensile strength of the bond be maintained as the compliant layer was built in. Thus many material combinations initially investigated proved unsuccessful (e.g. softer rubber or foam-backed carpet). Several types of adhesives were tried, but none was successful in making an intimate bond with the rubber layer, causing the laminated configuration to rupture at a very low tensile stress.

Subsequently the rubber layer was not used to determine if the carpet, when its jute backing was thoroughly permeated with epoxy, would give a suitable combination of compliance to shear stress and extension of the interface. Again a number of adhesives were tested and the best bond of all for this application was made with a Hysol Epoxy 0151, two-part compound. The setting period for the glue at room temperature is 10 to 12 hr, leaving ample time for the fluid mixture to soak into the weave of the carpet backing. Samples made with end caps having this epoxy-carpet face at no time exhibited the end zone fractures previously described. Working in conjunction with techniques of reduction in sample cross section and grain refinement in end zones, both of which will be discussed shortly, these modified end caps were very successful in transmitting tensile stress through the sample end zones, allowing fractures in the central section. While this design was employed in all end caps for tension, the simpler plucked end caps were used in compression samples (see Fig. 7).

Specimen production

The aluminum sample mold, end caps and associated parts for assembly were equilibrated in the 12.2 C coldroom where the preparation process was carried out. The inside surfaces of the cylinder halves, and the inside of the Lucite sleeve in the case of necked-down tensile samples, were smeared lightly with silicone grease to prevent adhesion of the frozen sample. The halves of the mold were then carefully fitted together with one strip of Teflon tape laid along the inside of each interface. As the tangential bolts and circumferential clamping rings were tightened firmly, the tape helped to form a vacuum-tight seal (see Fig. 8).

The outside faces of both end caps (i.e. the surfaces that would become the outer ends of the sample) were smeared with silicone grease to prevent ice adhesion, and the aligning rings were attached to these surfaces with three screws spaced around the perimeter. One of these prepared end caps was slid into place at the bottom end of the cylinder and fixed firmly there with radial screws extending through the cylinder wall and threading into the side of the ring. The heads of these screws were countersunk and seated on O-rings slightly wetted with vacuum grease to provide a tight seal. For necked-down samples, the acrylic sleeve was then inserted into the mold and each half was held in place with a screw extending in from the wall that was similar to those used to mount the end caps.

At this point the mold was packed with the seed grains of ice. The crystals were poured into the cylinder in eight layers, each layer being packed firmly with a circular tamping tool. For compression specimens, the entire sample was made from grains of the same size range. In tensile specimens,

Figure 7. Specimen end caps. Cap at left shows aluminum alignment ring fastened to top of cap; cap in center has modified surface where carpet is epoxied to end cap to enhance ice bonding; cap at right is one used in compression samples, showing roughened bonding surface

Figure 8. Specimen mold partly assembled. Note holes through which the cylinder halves are bolted together and strips of Teflon tape along edges of matching faces to provide a vacuum-tight seal.

Figure 9. Sample mold during evaluation freezing process. Mold with copper freezing coil standing between water supply tank (left) and −5°C glycol bath (right). Vacuum is applied through tube at top of mold, and water introduced through the tube at bottom.

a "refining" technique was used: 25 mm at each end of the mold was packed with very fine snow crystals sieved to between 0.42 and 0.83 mm, and the central region was filled with the appropriate larger seeds (except when the entire sample was seeded with the fine snow).

This technique of refining the grains in the ends of tensile samples was employed in an effort to ensure that fracture would occur in the central section of the cylinder. As a higher tensile strength was expected for a finer-grained aggregate, this concept seemed reasonable. It neither imposed a geometrical stress concentration nor caused a deviation from the uniaxial stress state in the center of the specimen. Important to note, however, is that, although this method was effective in dealing with problems in the stress field, it complicated the measurement of strain. Relative displacement of the end caps represented the strain in the fine-grained end zones superimposed on that of the actual test material in the central zone. The refining technique was used in conjunction with the dumbbell shape on samples made in the late stages of testing and having fine-grained gauge lengths of $d < 2$ mm. The end-refining method proved to be sufficient by itself on all larger-grained samples.

When the cylinder was fully packed with seeds, the top end cap was dropped into place and care was taken to make it sit flush on the seed crystals when in its proper position. This top cap was fixed in place in the same manner as the bottom cap.

The final step in the assembly process was to fit each end of the cylinder with a rubber stopper to complete the vacuum-tight seal. Each stopper had a segment of 6.4-mm-I.D. plastic tube fitted through it to allow access to the sample chamber for the evacuation and flooding systems. The exposed end of each tube was capped with a "quick-connect" valve for convenient sealed attachment.

The assembled mold was then transferred to a coldroom held at 0°C. Placed in an upright position, the sample chamber was connected to a vacuum system through the top access tube, the bottom access remaining sealed. The sample was evacuated to a pressure of not greater than 200×10^{-3} mm Hg and held there for not less than 2.5 hr in order to remove most of the gas from the chamber.

Following this phase, and with the vacuum maintained, distilled, degassed water that had been held in an air-tight tank at 0°C was introduced through the bottom access tube and allowed to percolate up through the compacted crystals. When the liquid level reached the top of the sample, the vacuum was disconnected and a drain hose open to atmospheric pressure replaced it. By regulating a feed valve the water head was kept high enough so that no air was let into the sample as the drain line was connected, and the flow rate was set to an estimated 0.5 $cm^3\ s^{-1}$. This slow flushing was maintained throughout the freezing process and served to carry impurities and dissolved gases out of the sample.

The mold was frozen by means of a coil of copper tubing wrapped around the cylinder and circulating glycol coolant from a constant temperature bath at −5°C. The sample mold during freezing is shown in Figure 9. The coolant circulation was begun as the water level reached the top of the mold.

This freezing method was designed to promote a cylindrical freeze front that travels radially inward from the mold wall and closes on the core of the cylinder. Inspection of partially frozen samples that were taken from the cooling coil confirmed that the unfrozen portion of the sample was a cylindrical core. Slow solidification in this manner allowed impurities to be kept ahead of the freeze front and continually flushed away, minimized freezing strains due to the phase change of trapped water, and produced a uniform polycrystalline specimen (Cole 1979). The normal time until flushing had stopped, indicating freezing to the core, was about 6 hr, giving an average radial freezing rate of 2.1×10^{-1} mm s^{-1}. The specimen was left in the cooling coil for at least 3 hr after flushing ceased to assure complete freezing. The mold was then removed to a room at -5°C where it was dismantled and the specimen extracted. The ice was inspected for quality and the dimensions of the sample were measured with vernier calipers.

For storage until use, the ice cylinders were wrapped in cellophane and sealed in a plastic bag with about one cup of crushed ice. This crushed ice helped to maintain a high water vapor pressure around the specimen to reduce sublimation. The sample was then sealed in a second plastic bag and left standing upright at -10°C. The practice was adopted of storing each cylinder before use for at least 24 hr but not more than 10 days, in order that any residual strains from molding might be relaxed, but long-term recrystallization or sublimation would be avoided.

Specimen quality

Several methods were used to characterize the ice specimens fabricated for testing. Measurements of the density of the material and its bubble content were made to quantitatively describe quality. Measurements of the eccentricity of the cylinders indicated the extent to which the molding apparatus produced specimens that would be well aligned under a uniaxial load. Thin-section analysis facilitated inspection of crystal structure. Following are more detailed descriptions of each of these methods of analysis.

Density was determined by an iso-octane displacement test performed at -5°C. The sample was weighed in air on a laboratory balance, then immersed in trimethylpentane of a known density and weighed with the same balance while suspended in the liquid. From these data, a volume and unit weight could be calculated. Iso-octane tests were carried out for 11 samples, all of which were made after the fabrication process had been refined to consistently produce acceptable test specimens. The mean of the density measurements was 0.9163 g cm^{-3}, with a standard deviation of 0.0004. The theoretical density of polycrystalline ice at -5°C is 0.9171 g cm^{-3}, based on a value at 0°C of 0.9164 g cm^{-3} and a linear thermal expansion coefficient of 52×10^{-6}/°C (Hobbs 1974).

Figure 10. Fine-grained specimen. Note the thin core of cloudiness extending along the axis

Upon visual inspection, fine-grained specimens were very clear throughout, except for a cloudy column about 10 mm in diameter which ran along the axis of the cylinder (see Fig. 10). This column is attributed to gas bubbles which were trapped as the freezing front encroached on the center of the cylinder.

Specimens with larger grains made from ice sheets had visible bubbles segregated at the grain boundaries, making the whole sample appear somewhat cloudy. Figure 11a shows a 5-mm-thick wafer of a sample, in which this condition was especially prevalent, exposed to oblique lighting to enhance the visibility of the bubbles. In order to put in perspective the extent to which the lighting

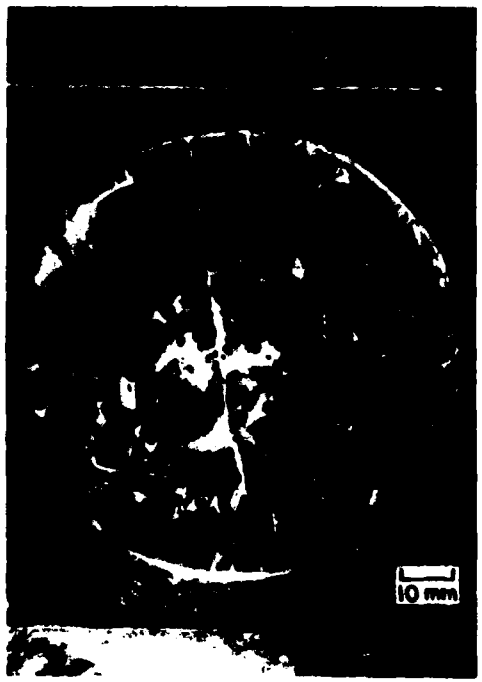

a. Coarse-grained ice wafer (5 mm thick) showing bubbles, especially those segregated at boundaries.

b. Fine-grained ice wafer (5 mm thick) showing bubbles (same as in Fig. 10)

Figure 11. Wafers of coarse-grained and fine-grained ice showing bubbles.

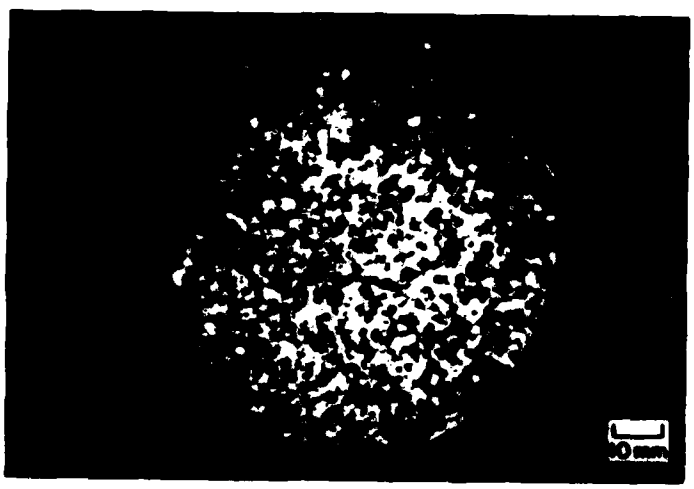

Figure 12. Thin section of a fine-grained specimen.

enhanced the effect, Figure 11b shows a similar view of the same sample that appears in Figure 10. The reason for the appearance of bubbles at the boundaries of the large grains is not understood. One line of reasoning is that the surfaces of ice grains that have been crushed from a sheet, as opposed to snow grains, offer sites that are energetically more favorable for nucleation of bubbles during freezing.

Bubble content was quantified by viewing wafers of ice under a microscope. The method was that described by DeHoff (1968) for characterization of a second phase dispersed in a matrix. Bubbles were assumed to be spherical, and the following equations apply:

$$N_v = 2N_a Z/\pi$$

where N_v is the number of spheres per unit volume of the phase being measured, N_a is the number of intersections a planar surface makes with the phase, per unit area, and Z is the reciprocal of the average intersection diameter. The average radius R of the spheres of the dispersed phase is given by:

$$R = \pi/(4Z).$$

The total number of bubbles intersected in a plane of focus of the microscope was counted, and the diameter of each intersection was measured according to a scale displayed across the field of view. Four samples were measured in this way, two fine-grained samples showing 1.5 bubbles mm^{-1} with a mean radius of 0.05 mm, and two coarse-grained samples giving 0.35 bubbles mm^{-1} with a 0.12-mm radius.

Eccentricity of a specimen was checked by mounting the cylinder in a comparator and spinning it on its axis while measuring relative deflection of a dial indicator set radially against its side. For spinning, the end caps of the samples were fitted with center-drilled, threaded (1 in.-14 threads) plugs for alignment in the same manner as the loading yokes for testing. While not every sample tested was checked for eccentricity, at least one sample made with each of the eight pairs of end caps was measured to make sure that all were consistent and that poorly machined or damaged caps were not used. The maximum dial gauge deflection measured on any of the samples was 0.56 mm, which, according to analyses used by Hawkes and Mellor (1972) and Haynes (1973) in their tensile experiments, translates to a maximum potential error in measured strength of 2.5%.

For crystallographic analyses of specimens, thin sections were made for viewing between cross-polarized sheets according to the procedure detailed in Appendix B. Figures 12-14 show cross sections of samples of small, intermediate, and large-grained samples. The equiaxed nature of the crystals and their uniformity can easily be seen by the contrast between grains. The random orienta-

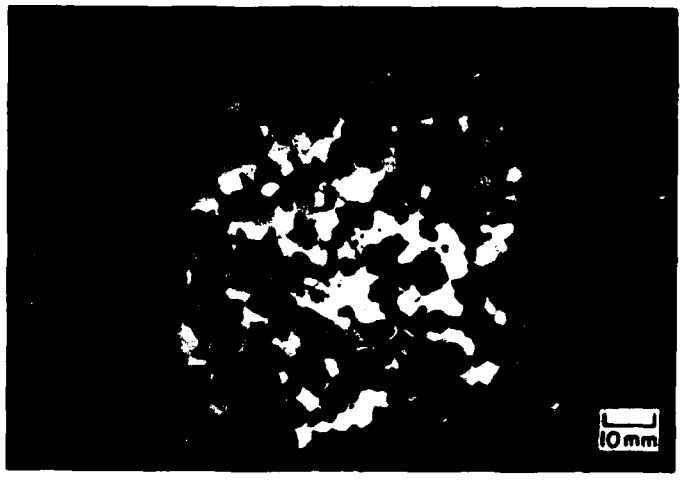

Figure 13. Thin section of a sample with intermediate-size grains.

Figure 14. Thin section of sample made with large grains.

Figure 15. Longitudinal thin section of large-grained sample with refined end zones, after fracture. Note equiaxed, randomly oriented crystal structure in this plane as well, sharp transitions between gauge length and fine-grained ends, and fracture through sample in gauge length.

tion is reflected in the varying brightness of the grains, as the amount of light that can pass through a polarizer, the specimen, and then the analyzer depends on lattice orientation of the ice (see App. B).

Figure 15 shows a longitudinal section of a sample that has been tested. The randomly oriented, equiaxed grain structure is seen to exist along the length of the sample. The sharp transition between the refined zones and the gauge length is also readily apparent.

The average grain size of the specimens was measured from thin sections by the line intercept method. Grain size determination was made immediately after a section was taken to avoid error from possible recrystallization or grain growth. To make the measurement, a line 80 mm long was laid across the surface of a section and the number of grains traversed by that line was counted. Five repetitions of this at five random orientations in the plane were made, and the total line length divided by the total number of grains crossed equaled the grain size, d. It is recognized that this method underestimates the actual grain size because most of the grains are intersected at less than their mean dimension. The extent of this underestimation is pointed out in Appendix A.

Tensile testing

Test equipment

Tests were carried out on a closed-loop electro-hydraulic testing machine (by MTS) with an environmental control cabinet between the crossheads. The bottom crosshead was fixed and loading was from a 98,000-N capacity actuator mounted on the top crosshead.

A major element in a tensile testing program for a brittle material is devising a loading train that applies pure uniaxial tension. Hawkes and Mellor (1972) and Haynes (1973) have dealt with direct uniaxial tensile testing of ice at CRREL and the former work presents a comprehensive review of other endeavors in the field. To the authors' knowledge, no technique has been developed to date which is entirely successful in applying pure uniaxial tension. Load alignment is a significant problem, which has been aggravated by freezing

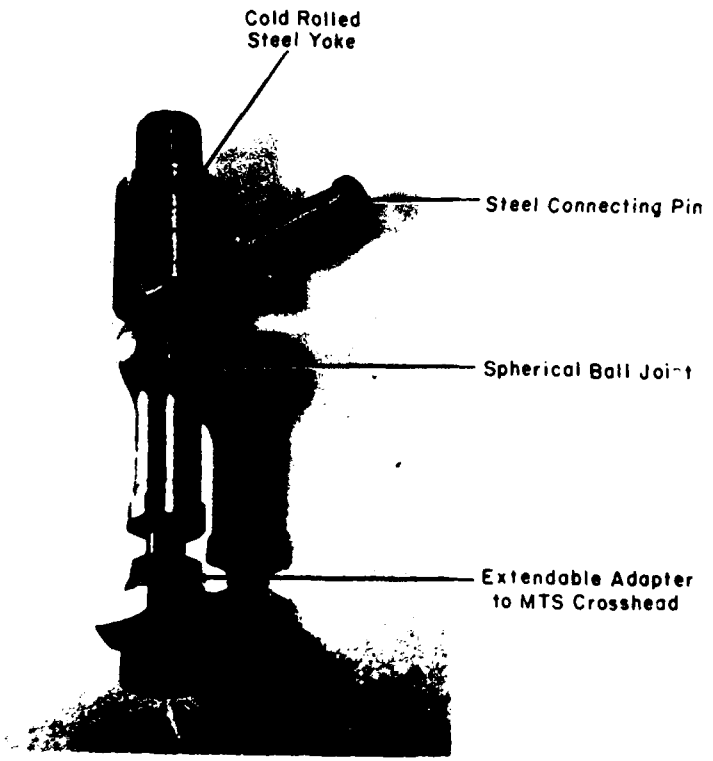

a. Tensile loading system which connects the specimen end cap to the testing machine crosshead.

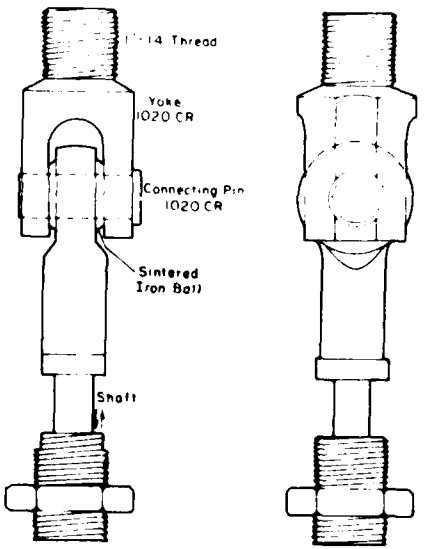

b. Two views at 90° rotation.

Figure 16. Tensile loading system.

the end caps onto the specimen after it has been formed. Cables used to load in tension have proven more compliant than is desirable. Fractures have most often occurred near the ends of the specimens, indicating that stress concentrations are introduced by the specimen geometry or the gripping method.

As no acceptable loading system was available, a device was designed and built to satisfy the requirements of this study. The design specifications of the tensile loading system were 1) that it apply only uniaxial tension to the specimen, 2) that it be compatible with the aligned end caps, 3) that it have a low compliance to minimize stored strain energy, 4) that it interface with the available testing equipment, and 5) that it allow quick setup and connection inside the environmental chamber to avoid thermal disturbances of the specimen.

The system developed is shown in Figure 16. A ball joint and yoke combination is used at each end of the specimen. The spherical ball joint is a component manufactured by the Split Ball Bearing Division of MPB Corporation, and is rated for a tensile force of 31.14 N (7000 lbf). In this ball joint a sintered iron ball rotates freely in a carburized steel race and has a 15-mm hole through its center where load may be applied. A yoke and pin, made of cold-rolled 1020 carbon steel, were machined for each ball joint such that the iron ball fitted snugly into the yoke and the pin slid through to make a rigid tensile connection. The shanks of the yokes were threaded (1 in.-14 threads) to turn directly into the holes in the specimen end caps. Connections were also made to adapt the ball joint shafts to 1 in.-14 threads so that they threaded into the MTS ram or bottom crosshead. The yokes allowed for specimen rotation in the horizontal plane. Also, up to 8° of specimen misalignment from vertical, even in the most restrictive direction, was possible. The device is simple and may be quickly mounted inside the environmental chamber.

The yokes were screwed into the sample end caps during preparation in a coldroom, and the ball joints fixed into the MTS crossheads prior to testing. A special feature was built into one of the ball joint connections (shown in Figure 16, and always used on the bottom in these tests) to allow for specimen setup without exact crosshead positioning. The adapter from the female thread inside the ball joint shaft to the 1-in.-14 male thread was of a variable length, having a shaft with a shoulder which slid inside the hollow, larger threaded section. This allowed about 20 mm of extension before the shoulder seated firmly against the end of the hollow shaft. Sample alignment consisted of simply lifting the top yoke into alignment with the ball on the top ram, and sliding the connection pin through both, then pulling the bottom ball into its yoke and pinning there. Any slack remaining in the system could be taken up by raising the actuator.

Load on the specimen was measured by a BLH 45-kN tension-compression load cell mounted on the bottom crosshead. It had the 1 in.-14 common threaded hole so that the loading train was screwed directly into it. The output was displayed on an oscilloscope for easy monitoring during testing as well as on a pressurized ink strip chart recorder. The load cell was calibrated on the testing machine and the calibration cell used was traceable to the National Bureau of Standards.

Specimen deformation during testing was monitored by two G.L. Collins SS-103 direct current displacement transducers (DCDTs) positioned along the specimen axis and diametrically opposed. A double clamp arrangement allowed axial displacement between the inner edges of the end caps to be measured. The DCDT barrels were fixed firmly to the top cap while the sliding cores rested on posts attached to the bottom cap (see Fig. 17).

The DCDTs were powered by a 6-V d.c. input and the two output signals were recorded on the strip chart alongside the load trace. Strain was calculated on the basis of the average of the output signals for most of the tests, and a single DCDT was relied upon in cases where one was not operational throughout a test. The procedures for calibration of the DCDTs is given in Appendix C.

Acoustic emissions generated by the specimen during deformation were monitored in many of the tests, allowing detection and recording of fracture activity prior to specimen failure. An acoustic transducer was placed in contact with the side of the specimen, as shown in Figure 17. Its signal was preamplified by 60 dB and band-pass filtered between 100 kHz and 300 kHz. Additional amplification brought the total gain to 88 dB. The signal was processed through a post-amplifier and an event counter for recording purposes. For further details of the acoustic emission detection system, the reader is referred to a recent work by St. Lawrence and Cole (1982).

Test procedure

Prior to testing, the ice specimens were taken from storage at −10°C and the threaded end cap holes and the sides of the end caps were scraped clear of ice. In order to remove surface defects

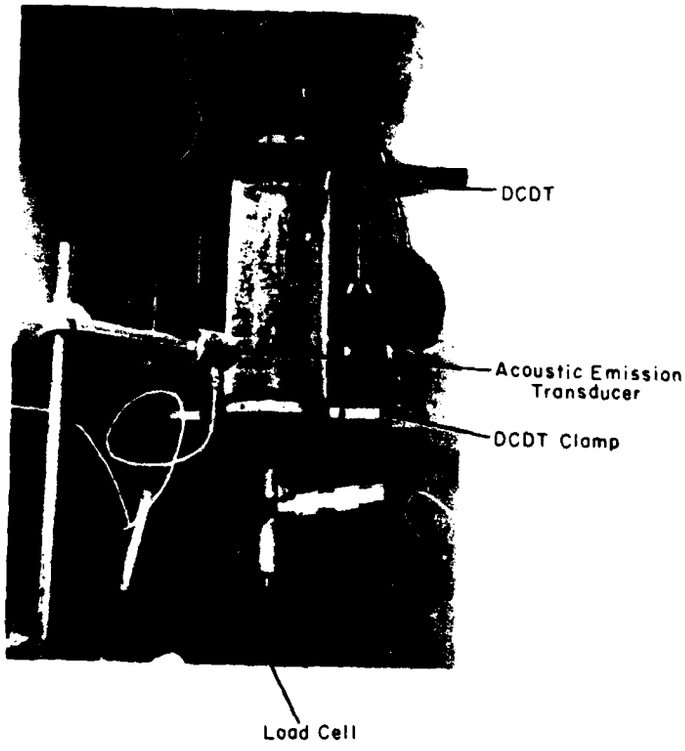

Figure 17. Tensile testing equipment in environmental chamber ready for testing.

relief caused by sublimation during storage, the specimens were rubbed firmly. Care was taken to give a uniform polish which resulted in a smooth surface over the length of the specimen.

Next the DCDT clamps were fastened on by circumferentially tightening screws and the transducer barrels and cores were put in place. The loading yokes were then screwed into the end caps firmly, with special care taken to hold the cap being fitted to avoid torsional loading of the ice.

The specimen was then quickly transported to the environmental testing chamber in an insulated box, where it was aligned in the loading train as described previously. The DCDT leads were connected by quick pin connectors to power and readout devices, and their initial output checked to be sure it was in the calibrated linear range. A thermocouple was placed in the cabinet near the sample to monitor temperature. All tests were carried out at $-10°C \pm 0.2°C$.

All tests were run at a constant machine speed of 2.3×10^{-4} cm s^{-1} which corresponds to a specimen strain rate of 10^{-3} s^{-1}. Because the loading system and end caps were not perfectly rigid, however, the strain rate that the specimen actually experienced was lower than this, as is discussed in *Experimental Results*. The actuator excursion was begun with a slight amount of slack in the system, and thus the initial load was zero. As the loading train reached its full extension the load rose slowly from zero and the test was begun. The load curve and DCDT outputs were recorded simultaneously on the strip chart. Acoustic activity was plotted against time on another chart alongside a duplicate load curve.

The strain rate and temperature regime used was not chosen for application to a specific problem, but rather because this regime was a reason-

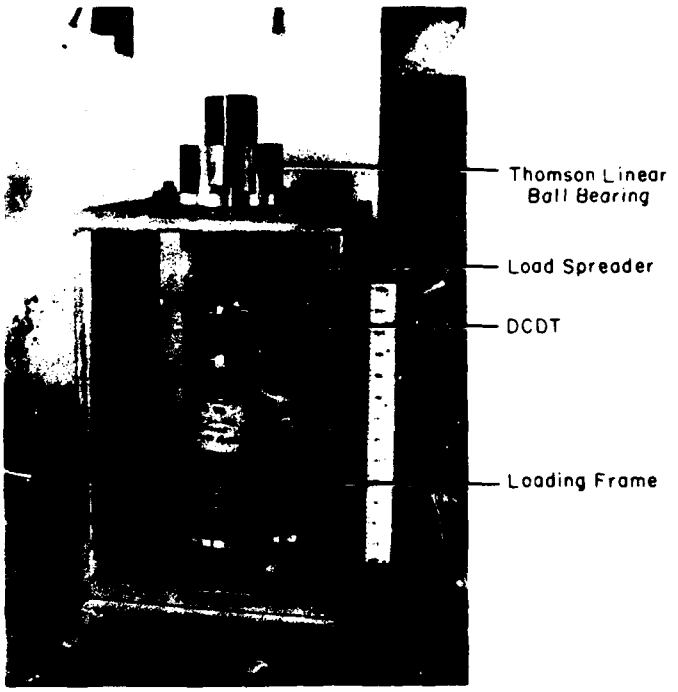

Figure 18. Compression test equipment.

able one in which to search for a B/D transition, and because those test conditions could be easily reproduced in subsequent experiments.

Compression testing

With the exception of the loading train, the equipment used for the few compression tests was the same as that used for the tensile tests. The DCDTs were mounted on the sample in the same way, but the load cell was mounted on the actuator above the sample instead of underneath as before.

The compressive load alignment system was that used by Pishvanov (1980). The sample sat flush on the base platform of a steel frame, and a shaft ran from the sample through a Thomson linear ball bushing bolted to the top of the frame. A conical section to spread the load was threaded into the end of the shaft, and this load spreader was threaded tightly into the top sample end cap. Load to the shaft was applied by the actuator through a spherical ball seat. Thus the force was transmitted through the Thomson bearing uniaxially to the specimen. The apparatus is shown in Figure 18.

As a sample was prepared, it was hand-polished in the same manner as for tensile tests, then set up in the compression frame in the coldroom. The sides of the open frame were fitted with insulated panels in order for the apparatus to be carried to the test chamber.

Tests were again carried out at -10°C and at a constant machine speed corresponding to a strain rate of 10^{-4} s^{-1} for the 23.1-cm specimen. The rate according to the DCDT output was less than that calculated from the machine speed, but this effect was not as pronounced as in the tensile tests.

Table 2. Tensile test data.

Test	Grain size (mm)	Time to failure (s)	Strain to failure (DCDT)	$\dot{\epsilon} \times t_f$ (crosshead)	Stress at failure (MPa)	Stress at onset of AE (MPa)	Total AE to failure*
27	5.9	346	0.0003	0.0035	0.864	—	—
31	5.8	342	0.0002	0.0034	0.864	0.339	30.8
32	4.6	332	0.0003	0.0032	0.881	0.305	23.8
33	3.6	342	0.0003	0.0034	0.898	—	—
34	1.1	400	0.0003	0.0040	1.186	—	—
38	1.0	376	0.0003	0.0038	1.186	—	—
39	1.4	390	0.0004	0.0039	1.186	—	—
40	3.2	386	0.0004	0	0.915	0.457	10.1
41	5.1	396	0.0004	0.0040	0.915	0.559	22.6
42	3.8	405	0.0005	0.0041	0.932	0.305	9.1
43	5.9	337	0.0002	0.0034	0.779	0.339	4.8
44	1.5	494	0.0013	0.0050	1.084	0.322	28.6
45	2.6	248	0.0002	0.0025	0.948	0.542	6.6
49	4.3	225	0.0002	0.0023	0.898	0.525	12.1
50	2.5	310	0.0005	0.0031	1.100	0.305	24.2
52	7.3	190	0.0002	0.0019	0.805	0.457	2.1
54 (N)	1.6	175	0.0004	0.0040	1.156	0.903	1.3
55 (N)	1.1	196	0.0007	0.0044	1.265	0.361	4.2

* Acoustic Emissions in terms of events cm^{-1}.
(N)—signifies necked specimen.

EXPERIMENTAL RESULTS

Tensile tests

The results of 18 tests are summarized in Table 2. Test conditions are constant throughout at a temperature of $-10°C$ and a machine speed of 2.3×10^{-4} cm s^{-1} (a strain rate of 10^{-4} s^{-1}). The grain size, as measured by the intercept method, was the variable parameter and ranged from 1.0 to 7.3 mm.

Failure occurred within the region of controlled grain size for all tests presented here. In all cases the fracture surfaces were perpendicular to the tensile axis and faceted (Fig. 19 and 20). Close inspection of the faces immediately after testing revealed that the mode of fracture in the larger-grained aggregates was primarily transgranular cleavage. The familiar streaks and dendritic patterns running away from the grain boundaries in the direction in which the crack propagated were readily apparent. In the finer-grained specimens, some cleavage features did stand out, but were not as extensive, possibly because each cleaved surface was much smaller than those with large grains. Replicas of three of the fractures were made by covering the surface with a solution of Formvar in ethane dichloride, allowing it to set, and melting the ice away. Examination of the replicas under a microscope and stereo-microscope (see Fig. 21) supported the observations mentioned above. Fracture of large grains was mainly by cleavage through the crystals but, as grain size decreased, some cleavage could be seen along grain boundaries where the break left rougher, but more uniformly textured facets. A complete characterization of the fracture mode for all grain sizes cannot be made without further analysis.

From the observed cleavage patterns, however, the crack path could usually be retraced to show the point of origin, and on a few of the samples two different points were found. Identified sites of fracture initiation were spread apparently randomly across the cross section and showed no correlation with the constant orientation of the loading yokes and ball joints.

It should be noted that early tests on relatively fine-grained samples (specimens 33, 34, 38, 39) were carried out with full cylindrical specimens having only slight grain refinement working to strengthen the end zones. Strain data for these tests could not be extended to later stages because of yielding in the carpet/ice interface region and weak epoxy bonding. However, the load continued to increase to the fracture stress listed, and these data were included because failure eventually occurred in the controlled grain size region of the cylinder. As the testing technique was refined, all end cap carpets were rebonded with the stronger epoxy, and very fine-grained samples were necked down in the controlled grain size re-

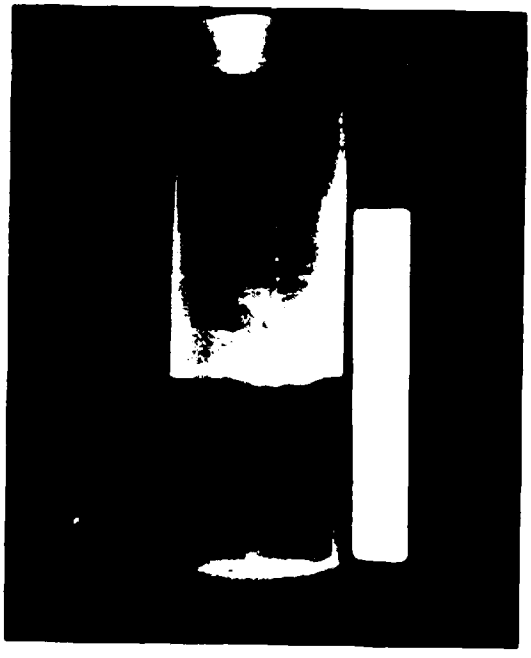

Figure 19. Full cylindrical specimen fractured in tension.

Figure 20. Tensile fracture surface revealing cleavage pattern.

Figure 21. Photomicrograph (26X) of cleaved ice surface. Note intersection of three grain boundaries in lower right and cleavage steps below grain boundary in upper left

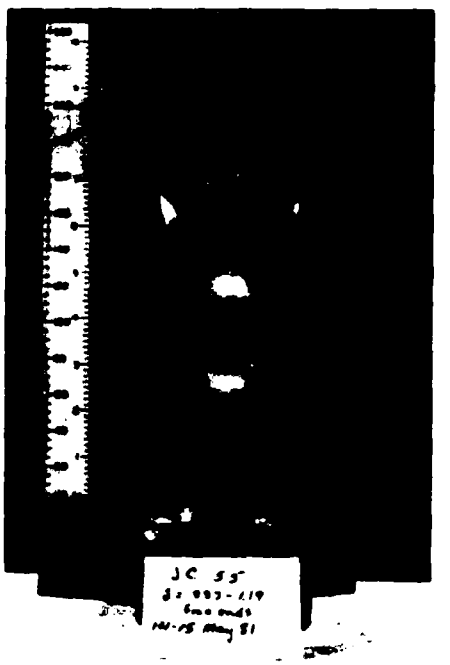

Figure 22. Fine-grained sample with reduced central section.

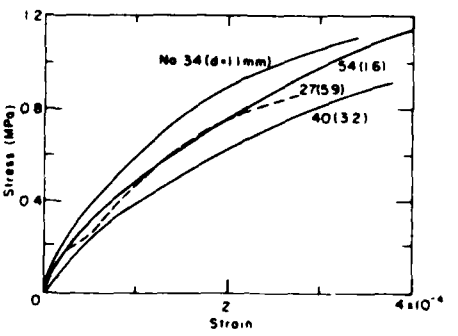

Figure 23. Stress-strain plots for tension tests.

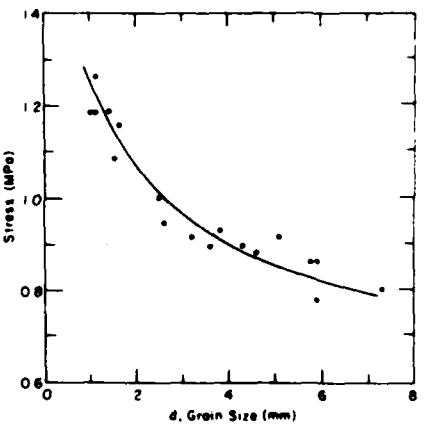

Figure 24. Tensile strength vs grain size.

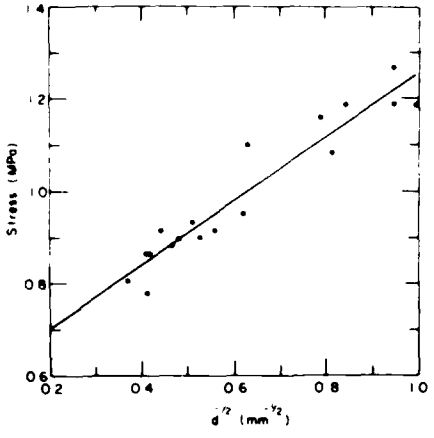

Figure 25. σ_f vs $d^{-1/2}$ for tension tests.

gion (specimens 54 and 55, see Fig. 22). This combination proved effective, as the 11 subsequent tests showed no end-failure problem.

The strain to failure given by the DCDT output is compared in Table 2 to the theoretical strain calculated by time to failure and crosshead speed. In general, the DCDT output is nearly one order of magnitude smaller, indicating that the samples actually experienced a strain rate of 10^{-6} s^{-1}.

Typical tensile stress-strain curves for four different grain sizes in the range tested are shown in Figure 23. All are quite similar in shape, steadily decreasing in slope until fracture. No clearly defined linear elastic portion of the curves can be discerned, which is a reasonable result for a viscoelastic material such as ice deformed at this rate.

The tensile test data are displayed in their simplest form in Figure 24 where fracture stress is plotted as a function of grain size. A marked grain size effect is readily seen, as stress to cause fracture drops significantly with increase in average grain diameter. This result is predicted where a fracture model based on dislocation theory is thought to be valid, as described below.

The question that now arises is: What functional relationship do the data obey? From Schulson's (1979) theory outlined above, two forms of equations predicted by the model are obeyed in the respective regimes where they apply:

$$\sigma_f = YK_{Ic}d^{-1/2} \tag{1}$$

which describes fracture stress if the material undergoes significant plastic flow before tensile failure, and

$$\sigma_f = \sigma_i + k_y d^{-1/2} \tag{2}$$

if fracture occurs at the onset of yielding.

To investigate these relationships, the fracture stress is plotted against the square root of the reciprocal of grain size in Figure 25. Inspection indicates a good straight line fit through the points. If consideration is first given to eq 1, it is seen that the failure stress should go to zero as d goes to a large value. However, the plot clearly shows that, although σ_f decreases with increasing grain size, the intercept at $1/d^{1/2} = 0$ is much greater than zero. Hence it is suspected that eq 1 does not adequately describe the data. Equation 2 predicts an intercept, which physically is the lattice's frictional resistance to slip. This quantity may be reasonably well estimated by considering the magnitude of the fracture stresses observed. It must be lower than the stress level at fracture of the largest-grained specimens tested (see Fig. 25) and, from the trend in the data, it may be assumed that the strength would be reduced to about 0.6 MPa when essentially no grain boundaries impede slip. This is consistent with the value of 0.8 MPa for single crystals presented by Muguruma (1969).

Now if eq 2 is restated and the logarithm of the expression taken,

$$\sigma - \sigma_i = k_y d^n \tag{3}$$

$$\log(\sigma - \sigma_i) = \log k_y + n \log d \tag{4}$$

a linear regression based on the data in terms of d and $(\sigma - \sigma_i)$, with σ_i taken as 0.6 MPa, will give explicit values for the Hall-Petch slope k_y and the exponent n. Such an analysis gives $k_y = 0.02$ MPa m$^{1/2}$ and $n = -0.51$, with a correlation coefficient of 0.92. This result is a strong indication that the fracture stress obeys the Hall-Petch relationship as theorized with a grain size dependence of $d^{-1/2}$.

Results of the acoustic emission monitoring indicated little or no cracking activity up to a certain stress, and then impulses were detected at an increasing rate as the load progressed upward to fracture. The environmental chamber had a window through which the sample could be observed during testing, and no visible cracks were observed prior to total specimen failure. The acoustic data for test 40 are plotted with the stress-strain curve in Figure 26 to show an example of how the number of events detected typically varied with deformation. The stress corresponding to onset of

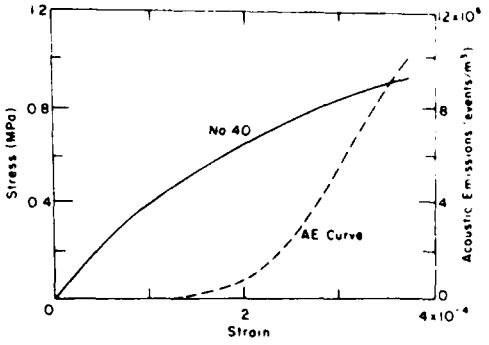

Figure 26. Tensile stress-strain curve plotted with acoustic emission data.

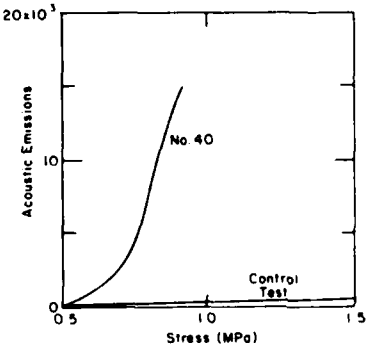

Figure 27. Acoustic emissions in a tensile test compared with AE in control test. Both are plotted against stress.

detectable acoustic activity was fairly constant for all tests in which end failure was not seen. The notable exception is test 54 in which onset came at 2 to 3 times the stress level of the other tests for an unknown reason. With this point included among the data, the mean value of stress at onset of emission is 0.436 MPa with a standard deviation of 0.163, or 37% of the mean.

In evaluating the acoustic data, a concern was that activity may have occurred within the epoxy bond and that this activity was responsible for some of the impulses detected. Two control tests were run in which the two end caps were bonded directly onto one another with the Hysol 0151, and were pulled in the normal fashion to a load of 11,120 N, exceeding all stresses reached in tests. In both trials the acoustic activity remained very near zero compared to that detected during actual testing. Figure 27 compares the number of acoustic events detected vs stress during a typical test with the number detected at the corresponding stress values in the control tests. It is concluded that essentially all of the acoustic emissions detected were generated only in the ice.

Compression tests

Five compression tests were carried out on specimens having a range of grain sizes from 1.1 mm to 6.3 mm. The primary purpose of the compression tests was to determine the yield strength of the material. This compressive yield strength could be compared to the tensile fracture strength to further test the theory of a B/D transition grain size. Of interest also were the ultimate strength data and the acoustic emission data obtained from the compression tests.

The results of four compression tests at a machine speed corresponding to a strain rate of 10^{-3} s^{-1} are presented as stress-strain curves in Figure 28. Actual strain recorded indicates that the samples underwent a strain rate of about 7.5×10^{-4} s^{-1}. A fifth test with d = 1.1 mm was loaded at a relatively high strain rate initially due to a machine malfunction, and a comparable stress-strain plot is not available. The specimen was reloaded at the normal strain rate of 10^{-3} s^{-1} and continued deformation to a maximum compressive load of 4.06 MPa.

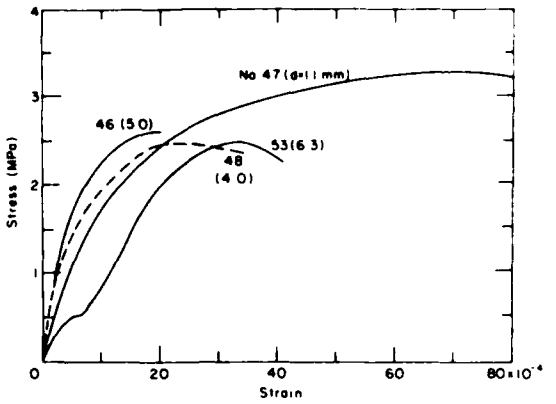

Figure 28. Stress-strain curves for compression tests.

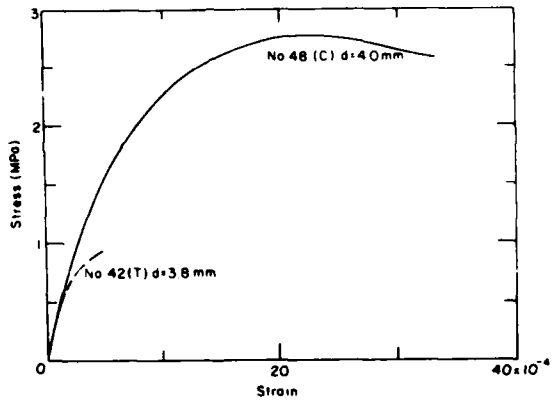

Figure 29. Tensile stress-strain curve plotted with compression stress-strain curve.

The compression tests were carried out to greater than 2% strain in each case, and maximum load occurred at 0.25 to 0.30% strain in three samples and at 0.70% strain in the fourth. This is a lower amount of strain for maximum stress than the value commonly found in other studies of around 1.0% (Hawkes and Mellor 1972, Mellor and Cole 1982).

The stress-strain curves show no consistent linear region to the onset of plastic strain from which yield stresses can be identified. The noticeable deviation from linearity appears to occur at a strain of approximately 2×10^{-4} and at a stress of 1 MPa for tests 46 and 48 (d = 5.4 and 4.0 mm respectively). However, the tests are too few to give reliable yield strengths, or to assess results relative to other work on the subject. Figure 29 shows a typical tensile stress-strain curve and a typical compression stress-strain curve plotted on the same scale for comparison.

The maximum stress achieved during compressive deformation was found to decrease consistently with increase in grain size. In keeping with the findings from the tensile strength data, the maximum stress in compression was plotted against $d^{-1/2}$, shown in Figure 30. The points for four of the tests are shown to be very nearly colinear, with the fifth test lying well below this line.

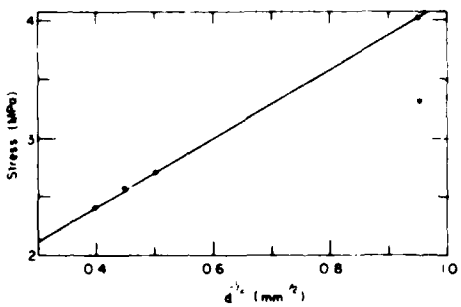

Figure 30. Maximum compressive stress vs d

Figure 31. Compression sample after test. Note that bulk of sample appears white as a result of fracturing

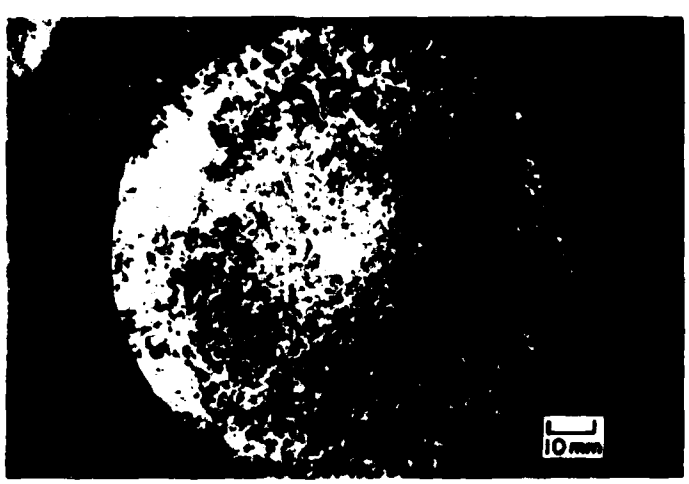

Figure 32. Cross section of a compression sample after test. Note abundance of cracks throughout.

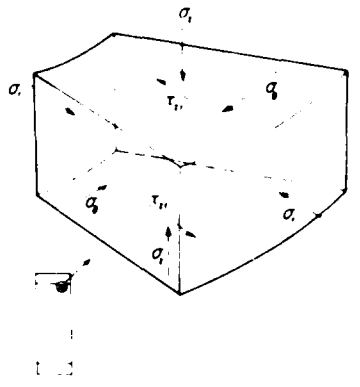

Figure 33. Stress state near end of sample during compression test.

Thus the analysis of the data was based on the former four points only. The slope of the line shown in Figure 30 is k_y, which is found to be 0.095 MPa $m^{1/2}$. This is in excellent agreement with the value of 0.097 MPa $m^{1/2}$ for columnar-grained ice with random *c*-axis orientation (Muguruma 1969).

Crack formation could be easily seen in the specimens during the tests. Cracks appeared abruptly with their surfaces at orientations within 40° of the specimen axis as far as could be established visually, and were not seen to propagate further after formation. In the compression test for which acoustic emissions were monitored, the first visual observation of cracking coincided closely with the beginning of acoustic impulse detection. This onset of cracking occurred at a stress of 0.34 MPa, a value near the stress at onset of acoustic impulses during tensile deformation. This is interesting to note since no visually observed cracks were produced during all acoustic emission prior to fracture in tensile specimens. The observation is that much larger cracks are formed in a compression test than in a tensile test at a given stress level. Further investigation of this phenomenon will not be discussed here, pending more test results to support the observation.

During the tests the specimens became cracked to the extent that they turned from transparent to white (see Fig. 31) and the cylinders became noticeably barreled. The acoustic activity accompanying strain to failure in the example seen was 53 events cm^{-3}, and the total of emissions to 2% strain was about 250 events cm^{-3}. The sample withstood many more fracture events in compression than in tension. A cross section of a strained compression sample is shown in Figure 32 where extensive cracking can be seen.

Cracking in the ends of specimens within 20 mm of the caps was suppressed and those regions remained clearer. It is proposed that the absence of a crack-inducing stress state in the end zones was due to a triaxial state of stress imposed by the end caps. This follows from an analysis presented by Hawkes and Mellor (1970) which shows that all stress components are compressive in a specimen near a restrictive end plane (see Fig. 33).

DISCUSSION

In discussing the significance of the findings of this study, it is helpful to review briefly the results achieved.

1. The uniaxial tensile fracture stress of the polycrystalline ice tested decreases with increasing grain size at −10°C and 10^{-3} s^{-1}.
2. The data fit the Hall-Petch equation, where σ_f varies as $d^{-1/2}$.
3. The apparent strength attributable only to frictional resistance of the lattice is 0.6 MPa.
4. The Hall-Petch slopes for tension and compression are 0.02 MPa $m^{1/2}$ and 0.10 MPa $m^{1/2}$, respectively.
5. Many microfracture events occur prior to tensile fracture.
6. The stress level at onset of acoustic emissions (with a gain of 88 dB) is roughly constant for tests of all grain sizes, and is about 0.4 MPa.
7. Although no definitive yield point was seen in the compression tests, acoustic emission data taken on one test show the onset of acoustic emissions at about the same stress level as for tension, and visible fractures accompany this onset.

Implicit in the achievement of reproducible tensile test results is the successful development of the testing technique. The system of carpeted end caps complementing grain refinement in the end zones of the sample and reduced cross section consistently resulted in fracture in the central region of the specimen. The yoke-and-ball joint loading train performed to specifications, being a very convenient device to use and giving no evidence of other than pure uniaxial loading.

The measured tensile strengths cannot be directly compared to any found previously, since no

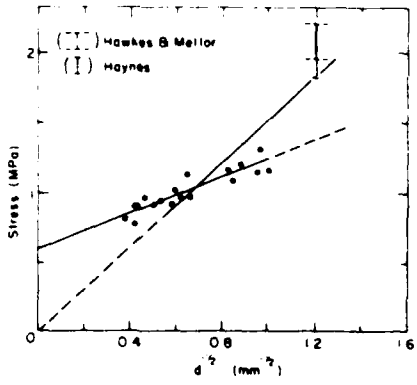

Figure 34. Current results (•) plotted with ranges of earlier data (from Hawkes and Mellor 1972, and Haynes 1973).

other tests on randomly oriented, equiaxed polycrystalline ice of these grain sizes have been carried out. Tensile strengths reported by Hawkes and Mellor (1972) and by Haynes (1973), all for ice of 0.7-mm average grain size as measured by the line intercept method, are shown with data from the present work in Figure 34. Results of Hawkes and Mellor were recorded at a test temperature of -7°C, and at a strain rate comparable to that experienced by the specimens in this study. Haynes' data are from -7°C and a strain rate of 10^{-4} s^{-1}. The tests run by Haynes were triaxial tests with a compression–tension ratio of 0.21. Although the current results show an increase in tensile strength toward smaller grain sizes, the data do not extrapolate to the other results shown. A consideration is that the transition to ductile behavior is predicted to lie at a grain size smaller than any of those tested here, and a corresponding increase in slope in the plot of σ_f vs $d^{-½}$ is expected. Whether this transition is manifested in the data for smaller grain sizes is yet a matter of speculation. The theory presented above suggests that

$$\sigma_f = 1.3K_{Ic}d^{-½}$$

in the ductile regime. Extrapolating this equation to a large value of d, the intercept on a σ_f vs $d^{-½}$ plot will pass through the origin. Based on this piece of information and the assumption that the higher fracture stress at a small grain size is in the ductile regime, the line on which fracture stresses of fine-grained ice would be expected to lie may be drawn. This line is included in Figure 34 to show where the data lie in relation to it. The indication is that the smaller-grain size data of the current work lie at stresses too low to substantiate this explanation. Making a determination difficult, however, is the sensitivity of ice to change in test temperatures in the range above -10°C, and possible sample size effects.

Considering that the tensile fracture stress data closely obey the Hall-Petch equation,

$$\sigma_f = \sigma_i + k_y d^{-½}$$

and that the expression derived from the fracture toughness concept,

$$\sigma_f = YK_{Ic}d^{-½}$$

does not adequately describe what is observed, it may be concluded that all of the fractures lie in the brittle regime. The fit is good evidence in support of the theory that brittle fracture stress varies as $d^{-½}$.

While it was hoped that the brittle/ductile transition at these test conditions would have been encompassed by the range of grain sizes used, practical constraints of sample size and seeds available have kept all grain sizes at $d > d_c$. Based on these test results, the indication is that, if smaller grain sizes are not achievable, the strain rate must be lowered or the temperature elevated to reach the B/D transition.

While it is recognized that the data cannot produce an intercept σ_i entirely independently of the grain size exponent n, a reasonably objective estimate was made at 0.6 MPa based on the trends seen. As stated earlier, this value agrees well with 0.8 MPa used in developing the quantitative theory (from Muguruma 1969).

Interesting results were seen in determining the Hall-Petch slope k_y. The compression data did reproduce very closely the value found in earlier compression experiments (Muguruma 1969), while the slope for tension was significantly lower. The values are 0.10 MPa m^{½} and 0.2 MPa m^{½}, respectively. The obvious question is: Why is there such a big difference between the Hall-Petch slopes for the two modes of deformation? With consideration of the processes involved, two answers to this question are proposed.

First, it is recognized that k_y for tension was obtained through a relationship of fracture stress to $d^{-½}$, and that stress occurred typically at strains of 3 to 4×10^{-4}. The value of k_y for compression, on the other hand, was based on the maximum stress

values achieved, and these were reached after considerably more strain, 2.5×10^{-1} at least. It is not clear whether the grain boundaries should be more or less effective in impeding slip propagation depending on strain; however, this may be a significant factor.

The second possibility has to do with the strength differential (SD) effect. In materials that exhibit this phenomenon, the yield stress in tension is lower than the yield stress in compression, and an analysis presented by Hosford and Allen (1973) shows that twinning and directional slip could be the underlying processes. Moreover, their model predicts that the effect would be seen in a randomly oriented polycrystal of an anisotropic material, which aptly describes the ice tested here. If, as according to the theory, shear in one direction occurs more easily than in the other, the effect of this on the Hall-Petch slope k_y can be identified by looking closely at the parameters that dictate slip propagation. Eshelby et al. (1951) show that

$$\tau_a^s = \tau_i + \langle m \rangle \left(\frac{Gb\tau_p}{\pi}\right)^{1/2} \ell^{-1/2}$$

where τ_a^s is the critical stress to cause dislocation slip. This expression is analgous to the Hall-Petch equation, where τ_i is the lattice's frictional resistance to slip resolved to a shear component, ℓ is the dislocation pileup length, and the coefficient of $\ell^{-1/2}$ is k_y in a basic form. In this coefficient, $\langle m \rangle$ is an orientational parameter for polycrystals, G is the shear modulus, b is the Burger's vector of the dislocations, and τ_p is the critical shear stress to propagate slip by boundary penetration. If the SD effect arising from directional slip is reflected totally in the term τ_i, then no difference in k_y will be seen. On the other hand, if the directional slip is manifested to some degree in the shear-related τ_p term, then a corresponding influence on k_y will result.

Which, if either, of the two proposed explanations for a differential in the k_y values is more likely cannot be decided here, nor can the magnitude of the effects be assessed. Further tests may produce better compression data at low strains that allow a comparison without the possible influence of strain on slip propagation or of the strength differential effect.

The theory reviewed in the *Background* section predicts that if the fractures in this series of tensile tests were of a brittle nature (occurring as plastic flow was beginning) the tensile strength should be equal to the compressive yield strength for the same material. From the limited compression data described here, a tentative estimate of the yield strength was made at around 1 MPa, which compares well with the tensile strengths. However, serious questions remain as to the reliability of the determination. It is best to look as well to other studies for data which may be applied.

Carefully controlled constant deformation rate compression tests have been carried out by Mellor and Cole (1982) on fine-grained ice. A characteristic common to all of the tests is a "knee" or local maximum in the stress-strain curve, as sketched in Figure 35. This was accompanied by a high rate of cracking as indicated by acoustic emission monitoring, and was identified as the yield stress for the material. The stress level at this yielding was 2.5 to 3.0 MPa for ice tested at -10°C and a strain rate between 10^{-1} s^{-1} and 10^{-4} s^{-1}. Clearly this indicates that fracture stresses near 1 MPa are occurring at a significantly lower level than that at which macroscopic yielding begins.

Although there is no doubt that the effect seen by Mellor and Cole is real and reproducible in their tests, consideration of the physical processes underlying it leads to the conclusion that this yield "knee" should not be interpreted as the onset of plastic flow. Since cracking activity has already begun, the dislocation theory of the fracture model says that dislocations have already been flowing extensively in the crystallites and have caused pileups significant enough to cause crack formation. In other words, the yield stress, as indicated by the beginning of plastic flow, has been reached and exceeded.

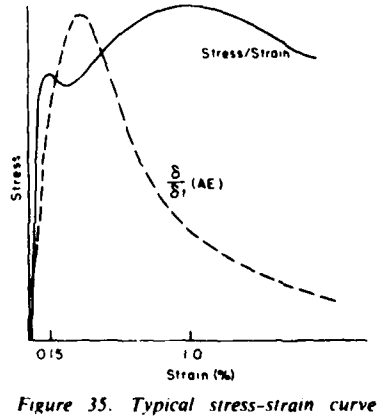

Figure 35. Typical stress-strain curve showing yield "knee" in compression, sketch of cracking rate shown alongside (Mellor and Cole 1982).

No fractures large enough to be seen were produced in the tensile tests, but acoustic impulses from some source were detected. Results of tests on commercial ice single crystals deformed in compression at −10°C and at stresses of 1 to 2 MPa show neither acoustic emissions (at a gain of 66 dB) nor visible fractures during deformation (St. Lawrence and Cole 1982). This indicates that the presence of grain boundaries is a major factor in producing emission-generating phenomena. As suggested by St. Lawrence and Cole, low energy (low amplitude) emissions may be generated by small intracrystalline fractures associated with low-angle grain boundaries. In addition, very high local stresses at the corners of faceted grains may, at very low strains, produce short cracks whose lengths may not necessarily reflect the size of the grains. There is yet much debate over the sources of low energy acoustic emissions detected during ice deformation.

With the limited data available, a sound judgment cannot be made regarding what the onset of acoustic emissions means in terms of the onset of yielding. However, the reproducibility of the tensile strengths and their agreement with the theory warrant a closer look at what the criterion for yielding should be.

As stated earlier, the strength differential effect could be a factor in the observed difference between tensile and compressive yield strengths. The ratio of the two in a hexagonal metal (zirconium) has been shown to approach a factor of two (Mannan and Rodriguez 1973). This information, in conjunction with the SD effect as it applies to the difference between k_y in tension and in compression, point to this area as one where further study may prove productive.

The acoustic data which have been presented here represent to the author's knowledge, the first such results for polycrystalline ice tested in uniaxial tension. To date, the premise has been that complete specimen failure would result from the first cracking event in a uniaxial tensile stress field (e.g. Michel 1978). Results of this study establish that an ice specimen will incur subcritical crack formation prior to failure, and that this activity is expected to begin at a stress level near 0.4 MPa.

CONCLUSIONS

The results of uniaxial tension and compression tests on polycrystalline ice with equiaxed, randomly oriented grains at a temperature of −10°C and a strain rate of 10^{-3} s^{-1} to 10^{-4} s^{-1} have yielded the following conclusions:

1. The ice specimen preparation technique used, as well as the tensile loading equipment developed, give reproducible results for uniaxial tensile tests.
2. A dependence of the tensile strength on average grain size exists in the range d = 1.0 to 7.3 mm, with grain size decrease resulting in strength increase. The grain size dependence of tensile strength is consistent with the Hall-Petch equation.
3. Significant acoustic emissions are generated in the ice prior to total specimen failure in tension.
4. Onset of acoustic activity at the 88-dB gain level occurs at about 0.4 MPa.

SUGGESTIONS FOR FURTHER WORK

1. Tensile tests over a range of strain rates would reveal the relative importance of strain rate to strength. These tests would assist in finding where the brittle/ductile transition lies in the temperature—grain size—strain rate relationship.
2. Similar tests performed at other temperatures would help the understanding of the effect of temperature on ice behavior. The range between 0°C and −10°C is one in which mechanical behavior is expected to be especially sensitive to temperature.
3. The occurrence of microfracture could be better characterized in future tests by incorporating an acoustic emission detection system capable of recording the amplitude distribution of impulses and estimating the location of the acoustic emission source in the specimen.
4. Strain rate in the uniaxial tests should be very closely controlled. Test techniques should result in the application of a truly constant strain rate, particularly at the start of the test.

LITERATURE CITED

Colbeck, S.C. and R.J. Evans (1973) A flow law for temperate glacier ice. *Journal of Glaciology*, 12(64): 71–86.

Cole, D.M. (1979) Preparation of polycrystalline ice specimens for laboratory experiments. *Cold Regions Science and Technology*, 1(2): 153–159.

Cottrell, A.H. (1958) Theory of brittle fracture in steel and similar metals. *Transactions of the Metallurgical Society of the American Institute of Mechanical Engineers (AIME)*, (4): 192–203.

DeHoff, R.T. and F.N. Rhines (1968) *Quantitative Microscopy*. New York: McGraw-Hill, pp. 128-148.

Eshelby, J.D., F.C. Frank and F.R.N. Nabarro (1951) The equilibrium of linear arrays of dislocations. *Philosophical Magazine*, **42**: 351-364

Gilman, J. (1958) Fracture of zinc-monocrystals and bicrystals. *Transactions of the Metallurgical Society of AIME*, **212**: 783-791.

Gold, L.W. (1972) The process of failure of columnar-grained ice. *Philosophical Magazine*, **26**(2): 311-328.

Gold, L.W. (1977) Engineering properties of freshwater ice. *Journal of Glaciology*, **19**(81): 197-212.

Goodman, D.J. and D. Tabor (1978) Fracture toughness of ice: A preliminary account of some new experiments. *Journal of Glaciology*, **21**(85): 651-660.

Hawkes, I. and M. Mellor (1970) Uniaxial testing in rock mechanics laboratories. *Engineering Geology* (Special Issue), **4**(3): 177-285.

Hawkes, I. and M. Mellor (1972) Deformation and fracture of ice under uniaxial stress. *Journal of Glaciology*, **11**(61): 103-131.

Haynes, D. (1973) Tensile strength of ice under triaxial stress. U.S.A. Cold Regions Research and Engineering Laboratory, Research Report 312. AD 774194.

Haynes, D. (1978) Effect of temperature on the strength of snow-ice. CRREL Report 78-27. AD A067583.

Hobbs, P.V. (1974) *Ice Physics*. Oxford: Clarendon Press.

Hosford, W.F. and T.J. Allen (1973) Twinning and directional slip as a cause for a strength differential effect. *Metallurgical Transactions*, **4**(5): 1424-1425.

Low, J.R. (1954) The relation of microstructure to brittle fracture. *Relation of Properties to Microstructure*. Cleveland: American Society for Metals.

Mannan, S.L. and P. Rodriguez (1973) Strength differential effect in zirconium alloys. *Scripta Metallurgica*, **7**(10): 1069-1074.

Mellor, M. and D.M. Cole (1981) Cyclic loading and fatigue in ice. *Cold Regions Science and Technology*, **4**(1): 41-53.

Mellor, M. and D.M. Cole (1982) Deformation and failure of ice under constant stress or constant strain-rate. *Cold Regions Science and Technology*, **5**(3): 201-219.

Mellor, M. and R. Testa (1969) Effect of temperature on the creep of ice. *Journal of Glaciology*, **8**(52): 131-145.

Michel, B. (1978) A mechanical model of creep of polycrystalline ice. *Canadian Geotechnical Journal*, **15**(2): 155-170.

Muguruma, J. (1969) Effects of surface condition on the mechanical properties of ice crystals. *Applied Physics (Journal of Physics D)*, Serial 2, **2**: 1517-1525.

Otten, G. (1972) Measuring water purity by specific resistance. *American Laboratory*, July.

Pishvanov, N.A. (1980) The influence of grain size on the creep rate of polycrystalline ice. Dartmouth College, Thayer School of Engineering, Bachelor of Engineering thesis (unpublished).

St. Lawrence, W. and D.M. Cole (1982) Acoustic emissions from polycrystalline ice. *Cold Regions Science and Technology*, **5**(3): 183-199.

Schulson, E.M. (1979) An analysis of the brittle to ductile transition in polycrystalline ice under tension. *Cold Regions Science and Technology*, **1**: 87-91.

Shoji, H. and A. Higashi (1978) A deformation mechanism map of ice. *Journal of Glaciology*, **21**(85): 419-428.

Smith, E. and J. Barnby (1967) Crack nucleation in crystalline solids. *Metallurgical Science Journal*, **1**: 54-56.

Weertman, J. (1973) Creep of ice. *Physics and Chemistry of Ice: Papers Presented at the Symposium on the Physics and Chemistry of Ice*. Ottawa: Royal Society of Canada, pp. 320-337.

Zaretsky, Yu.K., B.D. Chumichev and V.I. Solomatin (1979) Ice behavior under load. *Engineering Geology*, **13**: 299-309.

APPENDIX A: ADDITIONAL INFORMATION ON SEED GRAINS

Table A1 compares the average grain size d as measured by the line intercept method with the sieve windows from which the sample seeds came. Note that except for the very fine snow-grains, the d according to the intercept method was significantly lower than the average size of the sieves from between which the grains came.

As mentioned in the *Seed Grains* section, anomalous grain growth was seen in samples made from snow seeds of 0.42- to 0.83-mm diameter. The grain size as measured by the intercept method was 1.0 mm, significantly larger than the average of the seeds. Figure A1 shows a thin section of an untested sample made with these fine grains. The very fine crystals seem to have prevailed in the central region, but a wide perimeter shows significantly larger grains. One explanation is that many of the very tiny seed crystals melted during flooding, leaving fewer nuclei which then grew to correspondingly larger volumes.

Table A1. Average grain size compared with sieve windows from which seeds came.

Sieve sizes (mm)	*Avg d (mm)*	*Avg d seed*
0.42- 0.83*	1.0	1.60
0.83- 1.19	1.1	1.09
1.40- 1.70	1.4	0.90
1.70- 2.00	1.6	0.86
2.36- 4.00*	2.6	0.82
4.00- 4.76	3.4	0.78
4.76- 5.66	4.2	0.81
5.66- 6.30	4.5	0.75
6.30- 7.93	5.2	0.73
7.93- 9.52	5.9	0.67
9.52-11.20	6.3	0.61
11.20-12.70	7.3	0.61

* Large windows (see *Seed Grains* section).

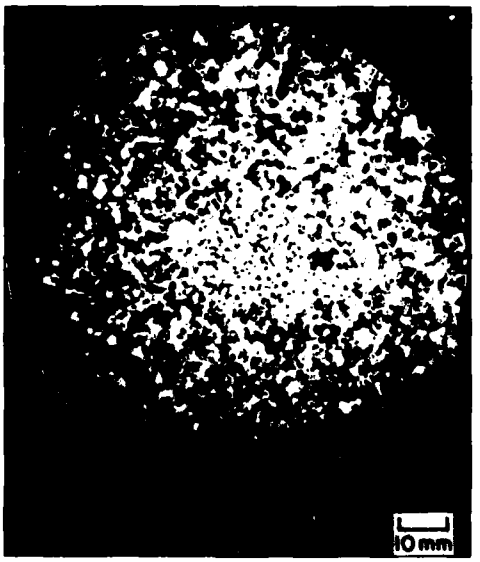

Figure A1. Thin section of untested fine-grained sample (seeds 0.42 to 0.83 mm).

After straining in tension, a sample made from the smallest seeds exhibited very significant grain growth near the end zones (see Fig. A2 and A3). These regions of grain growth seem to be hollow cones about 60 mm high, with their bases at the end caps, and having about the same diameter as the sample. This phenomenon, seen only in samples made of seeds 0.42–0.83 mm in diameter, is presumed to be caused by strain-induced recrystallization. The conical shape of the zone could be an indication of the way in which stress is distributed in the ends of the specimen, the recrystallized regions being those experiencing a higher stress and thus undergoing larger strains.

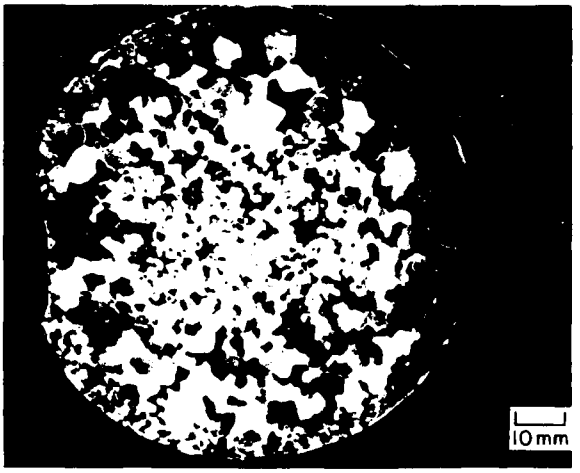

Figure A2. Cross section of fine-grained sample (seeds 0.42 to 0.83 mm) after test, section taken about 1 cm from end cap. Note large annulus where significant grain growth has occurred.

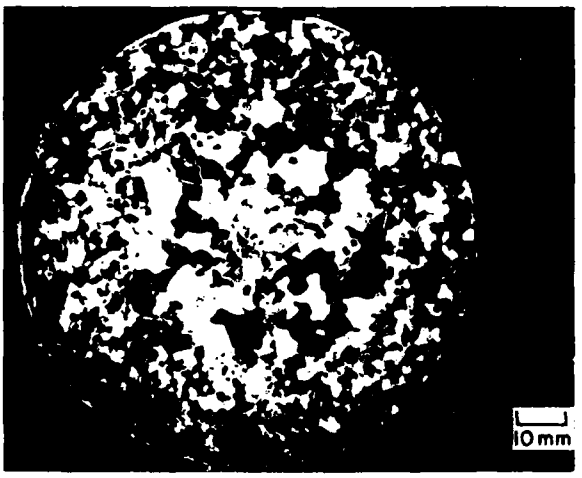

Figure A3. Cross section of fine-grained sample (seeds 0.42 to 0.83 mm) after test, section taken 3 to 4 cm from end cap. Note that annulus of enlarged grains is smaller than in Figure A2, reflecting conical shape of recrystallized region.

APPENDIX B: THIN-SECTIONING PROCEDURE

The entire process of thin sectioning a sample for analysis was carried out in a coldroom at −10°C. The plane of the sample to be investigated was exposed by cutting the specimen as smoothly as possible on a band saw. A common practice for convenient handling of the sample was to saw out a thick plate 1 to 2 cm deep with the plane of interest on one face. This exposed area was then flattened and polished by rubbing vigorously on a piece of carborundum mesh-screen lying on a smooth bench top.

A clean glass plate large enough to cover the polished surface was then chosen to support the thin section. The glass plates were cleaned with Micro brand liquid laboratory glass cleaner as experiments showed it to be quite effective in removing dirt and grease from the glass. Water would readily wet the surface without channeling or beading. A clean, easily wetting glass surface was found to be important in preventing entrapment of voids or bubbles as the specimen was frozen on.

The glass was placed on an electric hot plate that had been brought to a temperature quite warm to the touch. Immediately the polished surface of the ice sample was placed on the warming glass. Within a few seconds the ice/glass interface began to appear wet through melting of the sample, and very quickly the entire interface was liquid. As soon as this had occurred, allowing as little additional melting as possible, the glass and sample were removed from the hot plate and placed immediately on a cold aluminum block. The sample and the glass were always kept pressed together so that the liquid layer froze to bond the two firmly together without voids being introduced.

As soon as freezing was complete, the bulk of the sample was carefully sawed away on a band saw. A square fence was used on the saw table to guide the glass plate very closely to the blade, allowing the thin section remaining on the glass to be reduced to 3 mm or less in thickness.

In order to make the crystal structure of the sample clearly visible, the section was reduced in thickness even further using a microtome. The microtome is an instrument which has a smoothly sliding platform underneath a horizontally mounted razor-sharp blade. The platform rises, depending on adjustment, up to 20 μm each time it is pulled back and then pushed forward under the blade. The thin section was placed on the carriage with the glass side down and held in place either by means of a vacuum applied underneath it or by freezing a bead of water around the edges of the glass. The carriage level was then set so that the ice was nearly in contact with the blade and subsequent reciprocation of the sled shaved very thin layers off the section. The ice thickness was reduced in this manner to about 0.5 mm.

For viewing and analysis, the thin section on its glass mount was placed between crossed Polaroid sheets and illuminated with white light. In this configuration, each region of constant crystallographic orientation (i.e. each grain) had a different brightness and usually a different color than neighboring regions of different orientations. Hence the grain structure of the polycrystal in the particular plane of the section was easily seen.

The convenience of analysis by cross polarization of transmitted light is made possible by the fact that ice is a birefringent crystal. For an in-depth discussion of the optical properties of the material, the reader is referred to a text by Hobbs (1974).

APPENDIX C: DISPLACEMENT TRANSDUCER CALIBRATION

The displacement transducers (DCDTs) were calibrated at - 10 °C, according to a dial micrometer accurate to within 0.0025 mm. Power at 6-V d.c. was supplied by the same source used in actual testing, and output was read with a digital voltmeter. Calibration runs were made both with the core moving downward out of the barrel and upward into it, to simulate both tension and compression. The output for both modes was found to be a linear function of displacement if kept within the range of ±4 V, and all testing was carried out well within these bounds. Calibration data are tabulated in Tables C1 and C2 and plotted in Figures C1 and C2.

Table C1. Calibration data for DCDT S/N 180281.

Position (in.)	*Volts out (down)*	*Volts out (up)*
0.440	- 3.831	- 3.842
0.450	- 3.225	- 3.234
0.460	- 2.616	- 2.629
0.470	- 2.006	- 2.016
0.480	- 1.393	- 1.403
0.490	- 0.781	- 0.792
0.500	- 0.170	- 0.176
0.510	+ 0.445	+ 0.437
0.520	+ 1.058	+ 1.052
0.530	+ 1.671	+ 1.667
0.540	+ 2.285	+ 2.278
0.550	+ 2.896	+ 2.891
0.560	+ 3.503	+ 3.497
0.570	+ 4.108	+ 4.104

Table C2. Calibration data for DCDT S/N 197197.

Position (in.)	*Volts out (down)*	*Volts out (up)*
0.430	- 4.082	- 4.089
0.440	- 3.509	- 3.516
0.450	- 2.923	- 2.928
0.460	- 2.339	- 2.344
0.470	- 1.749	- 1.753
0.480	- 1.157	- 1.162
0.490	- 0.565	- 0.570
0.500	+ 0.027	+ 0.024
0.510	+ 0.617	+ 0.614
0.520	+ 1.207	+ 1.205
0.530	+ 1.797	+ 1.795
0.540	+ 2.383	+ 2.382
0.550	+ 2.964	+ 2.969
0.560	+ 3.548	+ 3.546
0.570	+ 4.120	+ 4.124

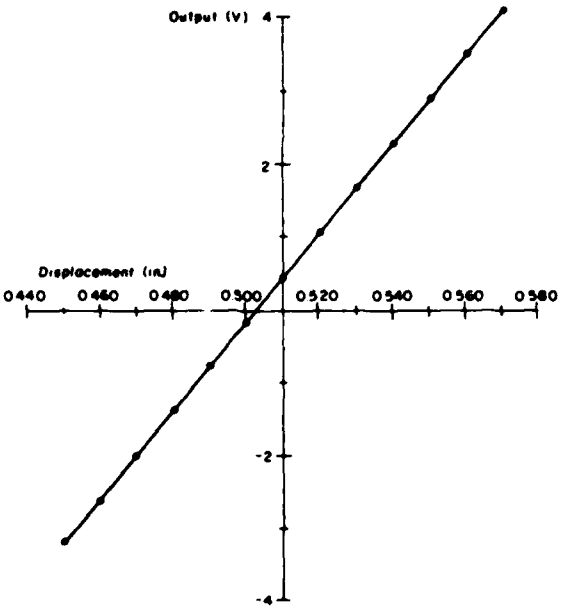

Figure C1. Calibration of DCDT S/N 180281.

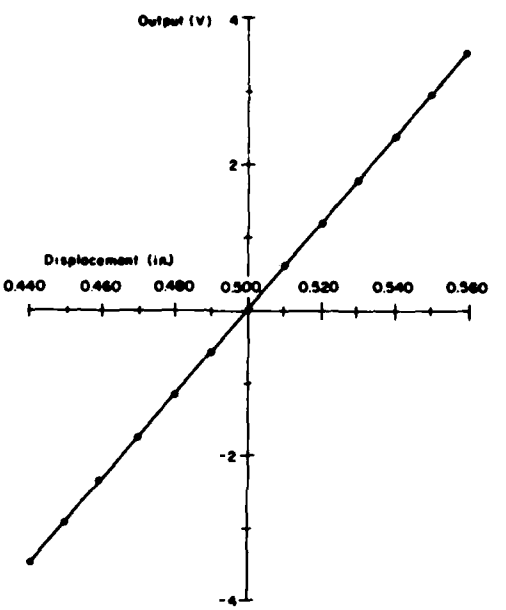

Figure C2. Calibration of DCDT S/N 197197.

A facsimile catalog card in Library of Congress MARC format is reproduced below.

Currier, J.H.
A study on the tensile strength of ice as a function of grain size / by J.H. Currier, E.M. Schulson and W.F. St. Lawrence. Hanover, N.H.: Cold Regions Research and Engineering Laboratory; Springfield, Va.: available from National Technical Information Service, 1983.
iv, 43 p., illus.; 28 cm. (CRREL Report 83-14.)
Bibliography: p. 30.
1. Ductile brittle transition. 2. Ice. 3. Polycrystalline. 4. Tensile properties. I. Schulson, E.M. II. St. Lawrence, W.F. III. United States. Army. Corps of Engineers. IV. Army Cold Regions Research and Engineering Laboratory, Hanover, N.H. V. Series: CRREL Report 83-14.

END

DATE
FILMED

2-83

DTIC